AD-A060 803 AERONAUTICAL RESEARCH LABS MELBOURNE (AUSTRALIA) F/G 11/6
RESIDUAL STRENGTH TESTS ON FATIGUE-CRACKED MULTI-FASTENER SPECI--ETC(U)
JAN 78 J Y MANN, F G HARRIS, G W REVILL

UNCLASSIFIED ARL/STRUC NOTE-444 NL

| OF |
AD
A060803

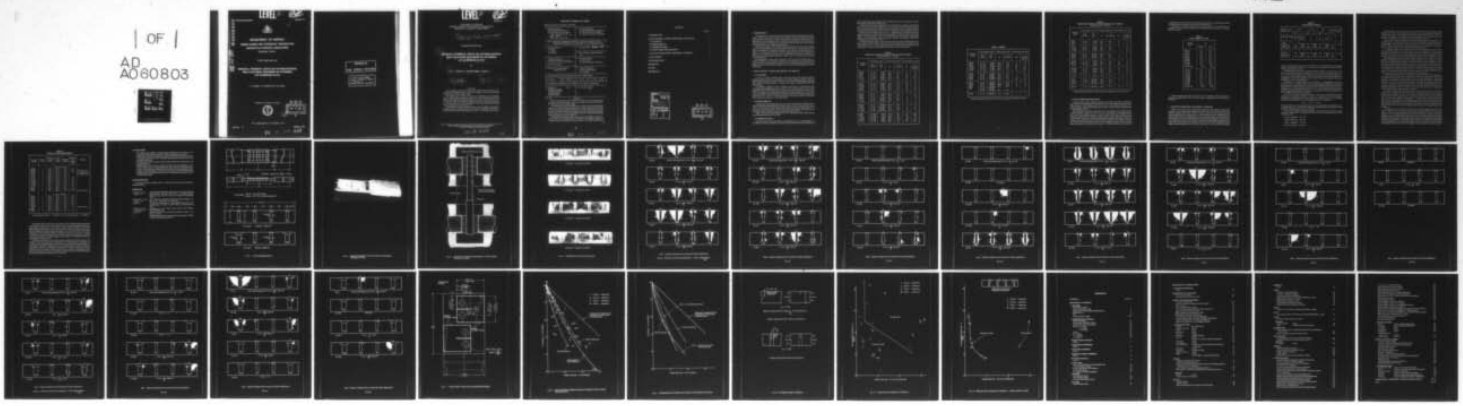

END
DATE
FILMED
01-79
DDC

ARL-Struc-Note-444

AR-000-1111

DEPARTMENT OF DEFENCE

DEFENCE SCIENCE AND TECHNOLOGY ORGANISATION

AERONAUTICAL RESEARCH LABORATORIES

MELBOURNE, VICTORIA

STRUCTURES NOTE 444

RESIDUAL STRENGTH TESTS ON FATIGUE-CRACKED MULTI-FASTENER SPECIMENS OF EXTRUDED L.65 ALUMINIUM ALLOY

J. Y. MANN, F. G. HARRIS and G. W. REVILL

Approved for Public Release.

COPY No 9

January 1978

LEVEL II

AR-000-1111

DEPARTMENT OF DEFENCE
DEFENCE SCIENCE AND TECHNOLOGY ORGANISATION
AERONAUTICAL RESEARCH LABORATORIES

ARL/STRUC NOTE-444

STRUCTURES NOTE 444

RESIDUAL STRENGTH TESTS ON FATIGUE-CRACKED MULTI-FASTENER SPECIMENS OF EXTRUDED L.65 ALUMINIUM ALLOY

by

J. Y. MANN, F. G. HARRIS and G. W. REVILL

44p.

Jan 78

SUMMARY

Static strength tests have been carried out on fatigue-cracked multi-fastener joint specimens of L.65 aluminium alloy to determine the influence of cracks of various shapes, sizes and locations on the residual strength.

The residual static strengths were found to be considerably less than would have been expected on a simple percentage loss-of-area basis; whereas simple fracture mechanics analysis using models of a semi-elliptical surface crack and a semi-circular corner crack at a hole consistently predicted lower failing loads than those obtained experimentally. For the larger crack sizes, the percentage differences between actual and predicted failing loads were greater than for small crack sizes.

Multiple fatigue cracking at different locations and the possibilities of interactions between cracks are complicating factors which introduce considerable uncertainties in extending simple fracture mechanics analyses methods to more complex practical cases.

POSTAL ADDRESS: Chief Superintendent, Aeronautical Research Laboratories,
Box 4331, P.O., Melbourne, Victoria, 3001, Australia.

DOCUMENT CONTROL DATA SHEET

Security classification of this page: Unclassified

1. Document Numbers (a) AR Number: AR-000-1111 (b) Document Series and Number: ARL—Structures Note 444 (c) Report Number: ARL—Struc.—Note—444	2. Security Classification (a) Complete document: Unclassified (b) Title in isolation: Unclassified (c) Summary in isolation: Unclassified

3. Title: RESIDUAL STRENGTH TESTS ON FATIGUE-CRACKED MULTI-FASTENER SPECIMENS OF EXTRUDED L.65 ALUMINIUM ALLOY

4. Personal Author(s): J. Y. Mann F. G. Harris G. W. Revill	5. Document Date: January, 1978 6. Type of Report and Period Covered: Note
7. Corporate Author(s): Aeronautical Research Laboratories	8. Reference Numbers: (a) Task: RD 73 (b) Sponsoring Agency: DST 76/155
9. Cost Code: 25 7020	
10. Imprint: Aeronautical Research Laboratories 1977	11. Computer Program(s) (Title(s) and language(s)): Not applicable

12. Release Limitations (of the document): Approved for Public Release

12-0. Overseas:	No.		P.R.	1	A		B		C		D		E	

13. Announcement Limitations (of the information on this page): No Limitations

14. Descriptors: Tests Mechanical Properties Cracking (fracturing) Fatigue (materials) Aluminium alloys	15. Cosati Codes: 2012 1113

16.

ABSTRACT

Static strength tests have been carried out on fatigue-cracked multi-fastener joint specimens of L.65 aluminium alloy to determine the influence of cracks of various shapes, sizes and locations on the residual strength.

The residual static strengths were found to be considerably less than would have been expected on a simple percentage loss-of-area basis; whereas simple fracture mechanics analysis using models of a semi-elliptical surface crack and a semi-circular corner crack at a hole consistently predicted lower failing loads than those obtained experimentally. For the larger crack sizes, the percentage differences between actual and predicted failing loads were greater than for small crack sizes.

Multiple fatigue cracking at different locations and the possibilities of interactions between cracks are complicating factors which introduce considerable uncertainties in extending simple fracture mechanics analyses methods to more complex practical cases.

A

CONTENTS

1. INTRODUCTION

A fundamental concept in fail-safe, damage-tolerant and safety-by-inspection design methods is that a structure must be able to maintain an acceptable level of static strength under specific loading conditions with some of its elements either broken or cracked. Thus, in addition to knowledge relating to crack propagation rates, it is essential to have information on the residual static strength of components containing cracks of different sizes. Relevant information is often obtained by conducting static tests on fatigue-cracked specimens.

A previous investigation[1] into the relative fatigue performance of various types of fastening systems for attaching sheet to heavy extruded sections involved tests on both continuous (full-sheet) and discontinuous (divided-sheet) specimens. For the full-sheet type specimens shown in Figure 1, it was found that about 90% of the final fatigue fractures occurred in an end row of fasteners. As the specimens were symmetrical in a lengthwise direction, it was considered that some fatigue crack development should have occurred in the row of fasteners at the opposite end of each specimen.

By conducting static tensile tests on the larger of the two previously broken pieces of a number of specimens, it was possible to determine residual failing loads, to clearly identify and measure the extent of fatigue cracking, and then to assess the residual strength of specimens with different numbers, sizes and shapes of fatigue cracks. The results of this investigation are outlined in this report.

2. TEST SPECIMENS, TESTING PROCEDURES AND RESULTS

2.1 *Test specimens*

A total of 57 broken specimens (Fig. 2) previously tested under axial-load constant-amplitude fatigue conditions[1] was available for this residual strength investigation. They had been manufactured from two batches of 100 mm by 32 mm British Standard BS L.64 aluminium alloy extrusion—designated BJ and CL—and precipitation aged to the requirements of BS L.65 before finishing.

The specimens included 38 Type E1 specimens which had No. 6 Parker-Kalon (PK) countersunk-head self-tapping steel screws at each of the 24 fastener locations, and 19 Type G specimens in which the No. 6 PK screws at the four corners were replaced by No. 12 PK screws. Of the 57 specimens, 34 were from material batch BJ and 23 from material CL. Prior to static testing the specimens were disassembled by removing all of the PK screws and the 16 gauge aluminium sheet "skin". However, no detailed inspection to detect fatigue cracking at the expected failure location was made prior to static tensile testing.

2.2 Residual strength tests

The previously broken fatigue specimens were held in hydraulic grips in a 600 kN Tinius-Olsen electro-hydraulic fatigue machine as shown in Figure 3. They were loaded in tension at a rate of 2·4 kN/sec, which resulted in failure after between about two and four minutes. A continuous trace recorder was used to record the load/time characteristics and failing loads, the latter being checked independently against a peak-load holding voltmeter.

Tables 1 and 2 give the static failing loads for the 57 specimens involved, together with the prior fatigue loading histories in each case.

2.3 Examination of fractures

After static testing, the fracture surfaces were examined at up to $\times 30$ magnification in a stereoscopic microscope to determine the extent of fatigue cracking. Because of the absence of

areas of rapid fatigue crack propagation and pseudostatic failure it was not difficult to identify the boundaries of the genuine fatigue cracks.

Of the 39 Type E1 specimens, eight either had no fatigue cracks or cracks so small that they were not detected at low power magnification ($\times 2$). Six of the 19 Type G specimens either had no cracks or very small cracks. The fracture surfaces of the 30 Type E1 and 13 Type G specimens which had well defined fatigue cracks at low power magnification were photographed at about $\times 1$ magnification, and enlarged prints made at $\times 2$ magnification. Some typical macrophotographs are illustrated in Figure 4. The areas corresponding to fatigue cracking on the fracture surfaces were then accurately traced from the photographs onto master sheets, making further reference to the actual fracture surfaces as required. A complete set of diagrams of the fatigue-cracked areas is shown in Figures 5 and 6.

Millimetre grid graph paper was used to determine the area of each individual fatigue crack. These values are noted on Figures 5 and 6, and the total cracked area for each specimen is also listed in Tables 1 and 2. It was considered that the error in the estimation of the total areas of *actual fatigue cracking* was less than 2 mm² for small areas and 2% for large areas.

TABLE 1
Detailed results of fatigue and residual strength tests, Type E1 specimens
Uncracked nett area = 1052 mm²

Specimen number	Prior fatigue stressing		Residual failing load		Total fatigue crack area	
	MPa nett area	Life, cycles	kN	% of uncracked*	mm²	% of uncracked nett area
BJ20D	79±159	8,300	379·5	69·3	137	13·0
BJ15C	79±159	8,500	504·0	92·0	41	3·9
BJ13I	79±159	8,700	392·5	71·7	136	12·9
CL25I	79±158	10,000	365·0	64·3	235	22·3
CL21C	79±157	10,600	497·0	87·6	66	6·3
CL22F	79±119	28,200	471·0	83·0	100	9·5
BJ18H	79±119	28,600	510·0	93·1	40	3·8
CL27G	79±119	31,400	423·0	74·6	125	11·9
BJ14F	79±119	33,500	479·5	87·6	46	4·4
CL26C	79±119	37,500	473·0	83·4	90	8·6
BJ18F	79±79	73,000	538·0	98·2	1	0·1
BJ12F	79±79	79,700	525·0	95·9	4	0·4
BJ16D	79±79	86,100	491·0	89·7	27	2·6
CL21I	79±79	103,000	512·0	90·2	35	3·3
CL24F	79±79	143,100	539·5	95·1	22	2·1
BJ19E	79±40	948,000	528·0	96·4	8	0·8
BJ20F	79±40	1,318,100	541·5	98·9	0	0
CL25G	79±40	1,504,000	515·5	90·9	50	4·8
CL24B	79±40	1,663,700	534·0	94·1	14	1·3
BJ4H	35±200	4,900	472·0	86·2	112	10·6
BJ7C	33±200	5,100	362·0	66·1	253	24·0
CL23G	32±199	6,000	442·5	78·0	98	9·3
BJ10F	33±203	6,800	409·5	74·8	168	16·0
CL21E	36±193	6,800	288·0	50·8	289	27·5

TABLE 1—continued

Specimen number	Prior fatigue stressing		Residual failing load		Total fatigue crack area	
	MPa nett area	Life, cycles	kN	% of uncracked*	mm²	% of uncracked nett area
BJ14B	32±139	25,500	495·0	90·4	31	3·0
BJ16J	32±139	27,400	509·0	92·9	36	3·4
CL26H	32±139	28,900	395·0	69·6	165	15·7
CL22H	32±139	33,000	384·0	67·7	137	13·0
CL23E	31±139	41,100	438·5	77·3	153	14·5
BJ1D	32±83	174,500	545·5	99·5	1	0·1
CL22J	32±79	257,000	556·5	98·1	2	0·2
BJ8H	32±83	262,800	526·5	96·1	15	1·4
BJ11E	32±82	309,000	409·0	74·7	130	12·4
BJ19C	32±63	506,000	551·0	100·6	0	0
BJ13C	32±63	658,000	460·0	84·0	59	5·6
BJ17I	32±63	905,000	549·5	100·3	0	0
BJ2I	32±66	2,585,400				
	32±82	440,200	554·5	101·2	1	0·1
BJ15I	32±52	4,486,000	552·5	100·9	0	0

* Taking "uncracked" BJ series as 547·5 kN and "uncracked" CL series as 567·4 kN.

TABLE 2
Detailed results of fatigue and residual strength tests, Type G specimens
Uncracked nett area = 996 mm²

Specimen number	Prior fatigue stressing		Residual failing load		Total fatigue crack area	
	MPa nett area	Life, cycles	kN	% of uncracked*	mm²	% of uncracked nett area
BJ11J	82±123	11,200	475·0	90·9	15	1·5
BJ20I	82±123	14,700	399·0	76·4	53	5·3
BJ17J	82±82	30,500	501·5	96·0	8	0·8
CL24H	82±82	35,900	518·0	95·7	7	0·7
CL23B	83±83	57,200	528·5	97·6	4	0·4
BJ15H	82±41	300,700	529·5	101·3	1	0·1
CL27E	83±41	425,500	532·0	98·3	0	0
BJ18E	83±41	1,199,700	521·5	99·8	0	0
BJ16E	32±123	21,400	375·5	71·9	37	3·7
BJ13D	32±123	25,100	428·5	82·0	39	3·9
CL21J	32±124	29,800	349·5	64·6	147	14·7
BJ19B	33±83	44,900	441·5	84·5	52	5·2
CL22E	33±83	56,200	464·5	85·8	68	6·8
CL21D	33±83	170,100	520·0	96·0	6	0·6
CL26I	33±66	93,700	551·0	101·9	0	0
BJ8I	33±42	889,700	498·5	95·4	16	1·6
CL25D	32±42	1,087,500	541·0	99·9	0	0
BJ14G	32±41	1,321,600	516·0	98·8	1	0·1
BJ12G	17±50	3,028,500	449·0	85·9	38	3·8

* Taking "uncracked" BJ series as 522·3 kN and "uncracked" CL series as 541·3 kN.

2.4 Fracture toughness and tensile properties

Compact tension fracture toughness specimens 25 mm thick were taken (as indicated in Fig. 7) from the end gripping portion of eight specimens used in the original fatigue investigation. These included six of the specimens used in the current residual strength investigation. The fracture toughness specimens were dimensioned and tested in accordance with the requirements of ASTM Standard E399–72.

During fatigue pre-cracking the maximum load of the fatigue cycle for individual fracture toughness specimens ranged from 6·3 kN to 7·8 kN, with a minimum load of approximately zero. The first four specimens (numbers CL26HS, CL29BS, BJ16JS and CL29BT) were pre-cracked in a 100 kN Amsler "Vibrophore" fatigue machine at a cyclic frequency of about 60 Hz. About 70,000 to 105,000 cycles were required to produce satisfactory cracks which, in these four specimens, were monitored optically. The remainder of the specimens were fatigue pre-cracked in a 330 kN MTS electrohydraulic machine at a cyclic frequency of about 30 Hz. For most of these, crack growth was monitored from the output of a COD gauge which also allowed the test

to be automatically discontinued when the appropriate crack length was reached. Between 43,000 and 78,000 cycles were required to pre-crack individual specimens.

The results of the fracture toughness tests are given in Table 3. It is clear that the CL material has a higher fracture toughness than does the BJ material, the average K_{Ic} value being about 20% greater.

TABLE 3
Fracture toughness of material

Specimen number	K_{Ic}	
	MPa m$^{\frac{1}{2}}$	ksi in$^{\frac{1}{2}}$
BJ15CS	25·9	23·6
BJ15CT	25·8	23·5
BJ16JS	25·9	23·6
BJ16JT	25·6	23·3
BJ18IS	26·8	24·4
BJ19BS	25·6	23·3
BJ19BT	25·8	23·5
Average	25·9	23·6
Std. dev.	0·41	0·37
Coeff. variat.	0·016	0·016
CL21CS	31·4	28·6
CL21CT	30·0	27·3
CL23GS	31·0	28·2
CL26HS	30·7	27·9
CL26HT	30·9	28·1
CL29BS	31·0	28·2
CL29BT	31·3	28·5
Average	30·9	28·1
Std. dev.	0·46	0·43
Coeff. variat.	0·015	0·015

Table 4 summarises the results of tensile tests on the two batches of material. Again the CL material has slightly higher proof and ultimate strengths—approximately 3% greater than the BJ material.

3. ANALYSIS OF FRACTURES AND RESIDUAL STRENGTH

Figures 5 and 6 show that, in many cases, fatigue crack development occurred simultaneously from a number of quite independent locations both within a particular fastener hole and also in adjacent fastener holes. The most common locations were the corners of the hole chamfers, the bottoms of the thread grooves cut by the self-tapping screws, unthreaded parts of the holes deeper than the self-tapping screws, and the drill-point regions at the bottom of the holes. However, there was a major difference in the fatigue crack development between the two types of specimens, in that most of the Type E1 specimens exhibited extensive crack growth from at least three of the fastener holes, whereas in about 75% of the Type G specimens the major fatigue cracking developed from one of the two outer holes. As a point of interest, the great

TABLE 4
Tensile properties of material

Material batch	No. of tests	0·1% PS		0·2% PS		UTS		Elong. (% on 2″)	0·1% PS / UTS
		MPa	psi	MPa	psi	MPa	psi		
Specification BS L.65 (minimum)		432	62,700			494	71,700	8	
BJ	25								
Average		457	66,300	463	67,200	510	74,000	11·5	0·90
Stand. deviat.		12	1,700	13	1,900	10	1,400	1·0	
Coeff. variat.		0·026	0·026	0·028	0·028	0·019	0·019	0·081	
CL	12								
Average		469	68,000	476	69,100	526	76,300	12·0	0·89
Stand. deviat.		9	1,300	9	1,300	6	900	1·0	
Coeff. variat.		0·019	0·019	0·019	0·019	0·011	0·011	0·076	

variety of fatigue crack initiation sites, crack shapes and sizes identified in these specimens emphasizes the problems which could be encountered in detecting and monitoring fatigue cracks by non-destructive methods.

It should be noted that, of the 57 specimens referred to in Tables 1 and 2, a total of 15 only were previously fatigue tested under conditions of either positive stress ratio (R) values or at $R = 0$. All of these had relatively long fatigue lives, and about 80% had fatigue-cracked areas of less than 5% of the original nett areas. Most of the specimens in which extensive fatigue cracking developed at the "residual strength" row of fasteners were tested at negative R values and had fatigue lives of less than 50,000 cycles.

Specimens with no fatigue cracks or very small cracks at $\times 2$ magnification, were used to assess the "100%" or uncracked strength of the two different types of specimens. For the Type E1 specimens the average failing load for specimens BJ18F, BJ20F, BJ1D, BJ19C, BJ17I, BJ2I and BJ15I was 547·5 kN. This compares with a value of 545·7 kN for the average failing load of two unfatigued Type E specimens from BJ material[1]. For the Type G specimens the average failing load for specimens BJ15H, BJ18E and BJ14G, and specimens CL27E, CL26I and CL25D are 522·3 kN (BJ) and 541·3 kN (CL) respectively.

As only one "uncracked" specimen from the CL material was included with the Type E1 specimens, the average failing load for the Type E1 CL specimens was calculated using the average ratio of the failing loads for Type G specimens in the two materials, i.e. 1·036. Hence the estimated average failing load for the uncracked Type E1 CL specimens was

$$547 \cdot 5 \times 1 \cdot 036 = 567 \cdot 4 \text{ kN}.$$

The ratio 1·036 is close to the value of the ratio of the average ultimate tensile strengths for the CL and BJ materials (i.e. 1·031), and this supports the method adopted for estimating the average failing load of the uncracked Type E1 CL specimens.

Values of the strengths of uncracked specimens, which were used as a datum for assessing the effects of fatigue cracks on the residual strengths of the various specimens listed in Tables 1 and 2, were thus:

Type E1, material BJ 547·5 kN

Type E1, material CL 567·4 kN

Type G, material BJ 522·3 kN

Type G, material CL 541·3 kN

Figures 1*b* and 1*c* show the cross-sections of the Types E1 and Type G specimens through the end rows of holes. In each case the uncracked nett area was calculated assuming hole diameters corresponding to those of the "tapping" drills, and allowing for the reduction in section area caused by the chamfers to accommodate the countersunk screws. The resulting nett areas were 1052 mm² and 996 mm² for the Type E1 and Type G specimens respectively.

Tables 1 and 2 indicate the failing loads of individual specimens as a percentage of the average failing loads of uncracked specimens, and the corresponding total fatigue-cracked areas as percentages of the uncracked nett areas. The results are presented graphically in Figure 8, where the three curves are best-fit second-order polynomial curves for the data on Type G specimens, a pooling of Types E1 and G specimens, and Type E1 specimens.

It is clear from Figure 8 that the failing loads of the fatigue-cracked specimens are much less than might be predicted on a simple loss-of-area basis; a finding which is in accordance with previously reported results shown in Figure 9 from static strength tests on fatigue-cracked bolted joints[2,3]. Figure 8 also shows that the percentage reduction in static strengths of Type G specimens are greater than those of Type E1 specimens with the same total fatigue crack areas.

Although fracture mechanics analyses have been successfully used to predict the residual strength of components with single cracks of simple geometric shape, the majority of crack cases which are illustrated for the Type E1 specimens in Figure 5 are not amenable to solution by currently available methods. However, for 11 of these specimens it was considered that the major fatigue crack development might be regarded as approximating to either a surface flaw or a single crack at the corner of a hole. In the Type G specimens, the majority of cracks initiated at the bottom of the screw head chamfer and it was not until such cracks propagated to the top surface of the specimen that they were considered to approximate to either a surface crack or a hole corner crack. Nine Type G specimens had cracks in these categories.

An attempt was made to predict the failing loads of these 20 specimens using, as appropriate, the fracture mechanics analysis for a semi-elliptical surface crack presented by Rooke and Cartwright[4] or the analysis for a semi-circular corner crack at a hole derived by Liu[5]. The idealised models are shown in Figure 10. The parameter K_0 used in the surface flaw model is a normalising parameter to account for particular crack boundary conditions, and numerical values of the ratio K_{Ic}/K_0 were determined from the nomogram given in Figure 186 of Reference 4. Table 5 summarizes the results of the fracture analysis of these 20 cracked specimens. The data are also presented graphically in Figure 11, where the chain dotted line simply serves to separate the results for the two types of crack geometries considered.

It is clear, for the particular types of specimens considered in this investigation, that the two fracture analysis methods both consistently predict lower failing loads than those obtained experimentally. In addition, the errors in the predicted failing loads appear to become greater as the crack size becomes larger. However, only eight of these 20 specimens strictly represented cases of single crack configuration development, or contained other small secondary cracks which were not considered to interact significantly with the major crack. The relevant specimens were Type E1 numbers BJ19E, CL25G, CL24B, BJ8H, BJ11E; and Type G numbers CL21J, BJ8I and BJ12G. The data for these specimens are reproduced in Figure 12 which gives more particular support, for the hole corner cracked specimens at least, to the general trend noted in Figure 11.

This behaviour may be associated with the extent of the plastic deformation at the tips of cracks of different size. During constant-load amplitude fatigue cycling the maximum stress intensity at the tip of a growing fatigue crack will progressively increase as the crack size becomes larger and, as a consequence, greater plastic deformation or blunting of the crack tip would be expected at the tip of a large crack compared with a small crack. Such blunting could increase the effective fracture toughness of the material compared with the value determined in accordance with the relevant Standards for measuring fracture toughness. For example, one of the ASTM Standard requirements[6] for a valid fracture toughness test is that the plane strain stress intensity corresponding to the maximum force of the fatigue cycle must be equal to or less than $0{\cdot}60\ K_{Ic}$.

TABLE 5
Summary of residual strength predictions

Specimen number	Method (ref.)	Predicted strength (kN)	Actual strength (kN)	Predicted / Actual	Maximum stress intensity (K_f)*	Remarks
			Type E1 specimens			
BJ20D	4	263·0	379·5	0·69	24·7	
BJ18H	4	378·4	510·0	0·74	14·2	For larger crack
BJ16D	4	405·9	491·0	0·83	9·8	For larger crack
BJ16D	5	406·6	491·0	0·83	—	For smaller crack
CL21I	4	469·4	512·0	0·92	—	
CL21I	5	343·0	512·0	0·67	15·0	
BJ19E	5	406·6	528·0	0·77	8·0	
CL25G	5	296·7	515·5	0·58	13·0	
CL24B	5	396·1	534·0	0·74	9·8	
CL26H	4	299·5	395·0	0·76	18·6	
BJ8H	5	352·2	526·5	0·67	8·9	
BJ11E	4	256·7	409·0	0·63	12·2	
BJ13C	5	241·5	460·0	0·52	10·8	For larger crack
			Type G specimens			
BJ11J	5	314·9	475·0	0·66	16·9	
BJ20I	5	249·0	399·0	0·62	21·4	
BJ16E	5	266·2	375·5	0·71	15·0	
BJ13D	5	257·2	428·5	0·60	15·6	
CL21J	4	261·6	349·5	0·75	18·4	
BJ19B	5	257·2	441·5	0·58	11·6	
CL22E	4	408·7	464·5	0·88	8·7	For larger crack
BJ8I	5	314·9	498·5	0·63	6·1	
BJ12G	5	266·2	449·0	0·59	6·5	

* For BJ material, 0·60 K_{Ic} = 15·5 MPa m$^{\frac{1}{2}}$; for CL material, 0·60 K_{Ic} = 18·5 MPa m$^{\frac{1}{2}}$.

The relevant values of the maximum stress intensities (K_f) for the largest fatigue cracks in each of the specimens listed in Table 5 were calculated using the same fracture analysis methods as those referred to previously. In seven instances, namely specimens BJ20D, CL26H, BJ11J, BJ20I, BJ16E, BJ13D and CL21J, the nominal calculated maximum stress intensity at the crack tip at the completion of fatigue cycling either exceeded or was very close to the limit of the ASTM requirements. These particular specimens are identified by small arrows on Figure 11. A further consideration is the rate of loading during the residual strength test in relation to those specified in the relevant Standards for fracture toughness determination. In this investigation, they were comparable to the specified values.

In addition to the severity of the original fatigue loading history having an effect on the sharpness of the crack tip and partly invalidating the use of the Standard K_{Ic} values, there are a number of other complicating factors associated with the prediction of residual strengths. For the particular configuration of specimens used in this investigation, three of the most important would appear to be, firstly, uncertainties in extending the two simple analytical stress analysis methods to the more complex sectional shapes involved; secondly, in recognizing the multiplicity of crack initiation sites both in and between specimens and, thirdly, in making allowances for interactions between both adjoining and remote cracks.

4. CONCLUSIONS

1. The residual static strengths of fatigue-cracked multi-fastener joint specimens is considerably less than would be expected on a simple percentage loss-of-area basis.
2. Simple fracture mechanics analysis using models for a semi-elliptical surface crack and a semi-circular corner crack at a hole consistently predicted lower failing loads than those obtained experimentally.
3. The differences between the actual and the predicted failing loads become greater with increasing crack size.
4. Multiple fatigue crack initiation at different locations and the possibilities of interactions between cracks are complicating factors which introduce considerable uncertainties in extending simple fracture analysis methods to more complex practical cases.
5. The great variety of fatigue crack initiation sites, crack shapes and sizes identified in these specimens emphasises problems which can occur in detecting and monitoring cracks by non-destructive methods.

ACKNOWLEDGMENT

The authors' thanks are extended to Mr. A. S. Machin for his assistance with the fracture mechanics analyses.

REFERENCES

1. Mann, J. Y., and Harris, F. G. — An investigation of the fatigue performance of three types of aircraft skin/spar boom fastening systems. Part 1: Constant-amplitude fatigue tests. *Rep. Aero. Res. Labs* No. ARL/SM 350, September 1974.
2. Kirkby, W. T., and Eynon, G. R. — The residual static strength of a bolted joint cracked in fatigue. *Tech. Rep. R. Aircr. Establ.* No. 66111, April 1966.
3. Darts, J. — The residual static strength of a fatigue-cracked bolted joint in an aluminium alloy. *Tech. Rep. R. Aircr. Establ.* No. 76156, November 1966.
4. Rooke, D. P., and Cartwright, D. J. — *Compendium of stress intensity factors.* London, Her Majesty's Stationery Office, 1976.
5. Liu, A. F. — Stress intensity factor for a corner flaw. *Engng Fract. Mech.*, vol. 4, 1972, pp. 175–179.
6. — — Standard method of test for plane-strain fracture toughness of metallic materials. ASTM Standard E399–74.

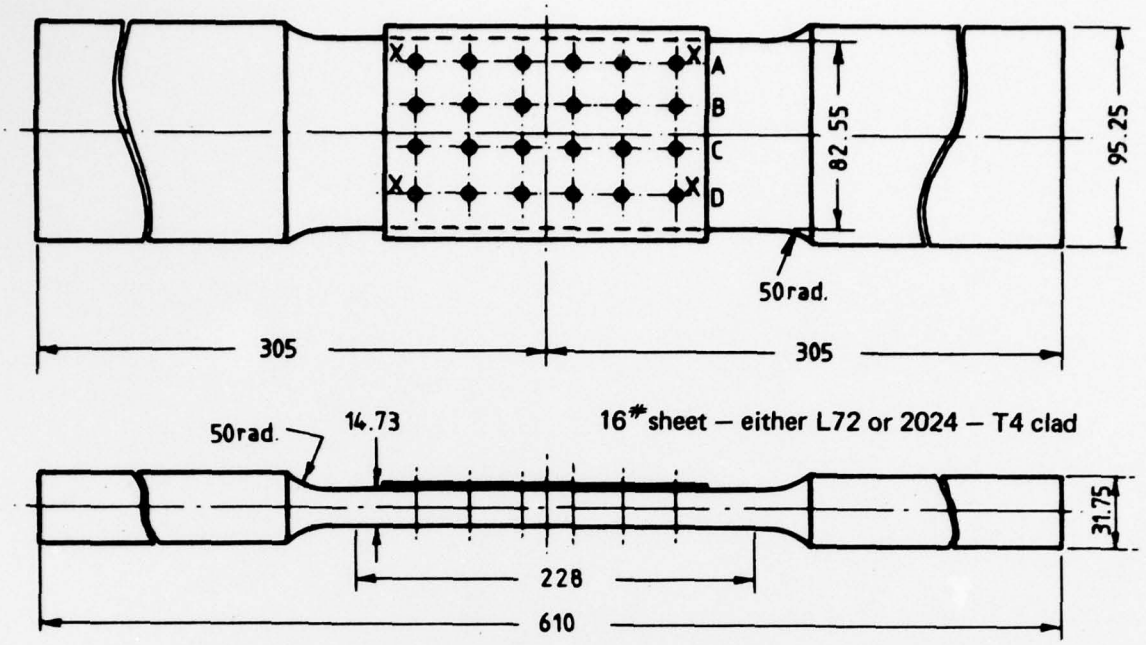

(a) Full sheet Type E1 – No. 6 P.K. screws
Type G – No. 12 P.K. screws at positions 'X'

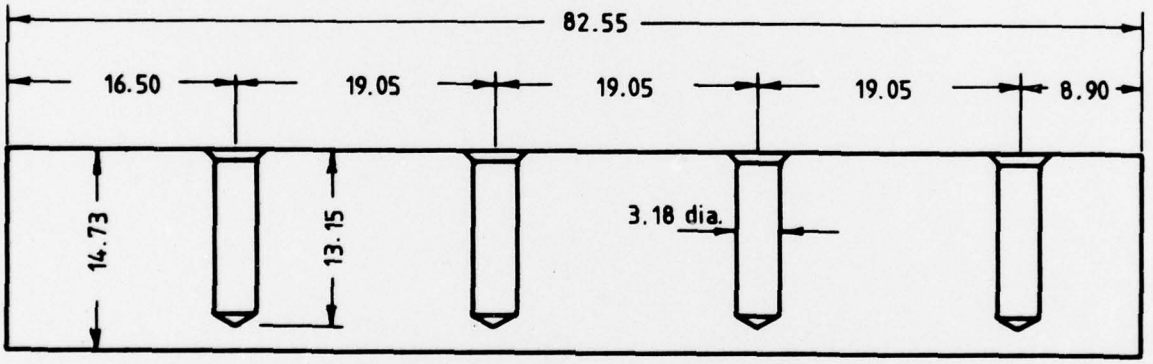

(b) Type E1 Nett area = 1052 mm^2

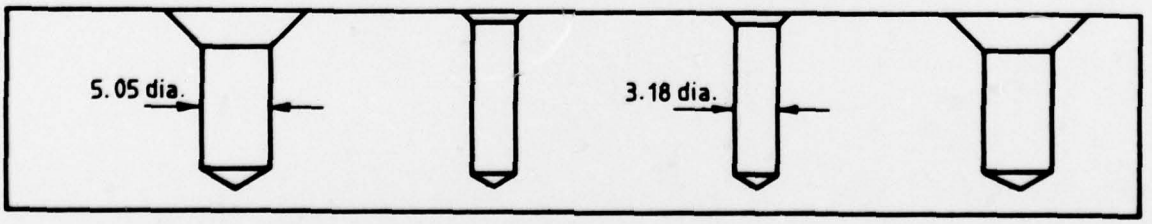

(c) Type G Nett area = 996 mm^2

FIG. 1 TEST SPECIMENS (Ref. 1)

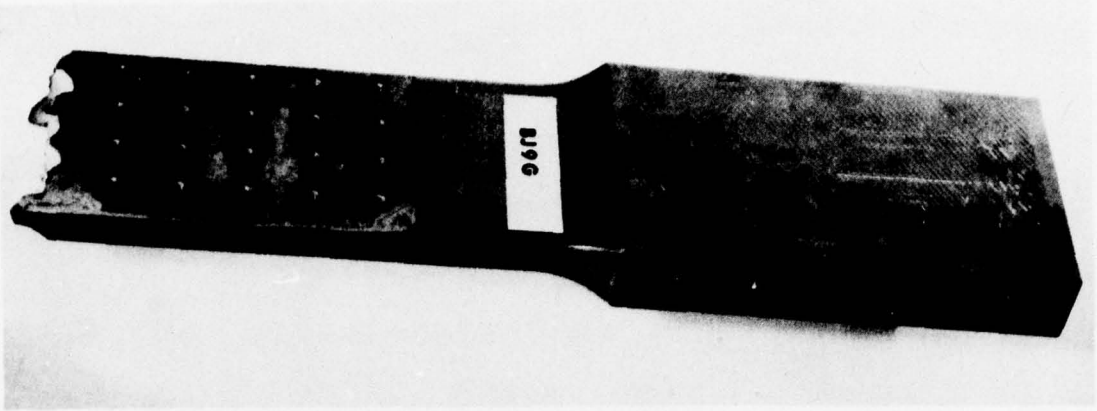

FIG. 2 BROKEN SPECIMEN (TYPE E1) USED FOR RESIDUAL STRENGTH TESTS

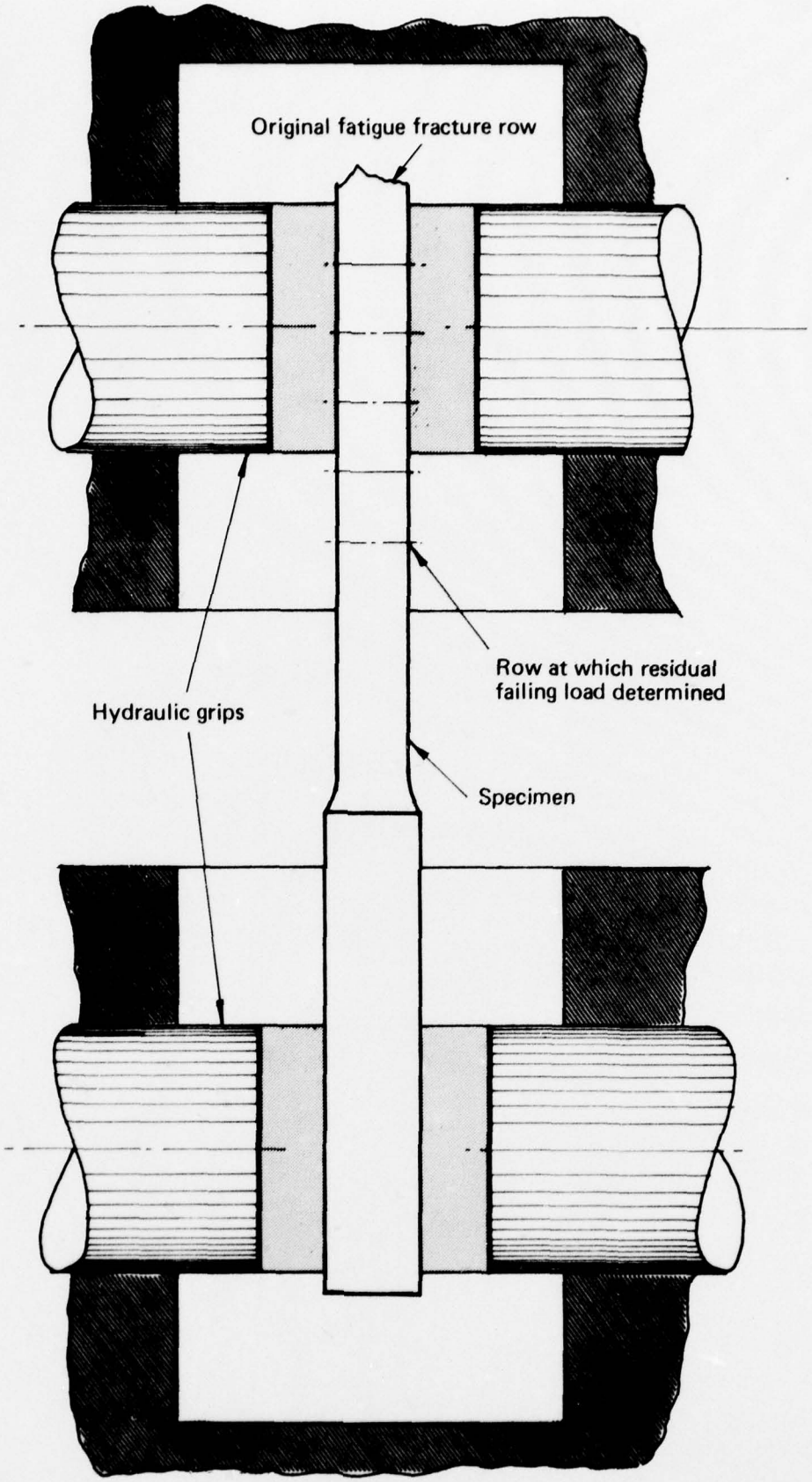

FIG. 3 MOUNTING OF BROKEN SPECIMEN IN TINIUS OLSEN HYDRAULIC GRIPS

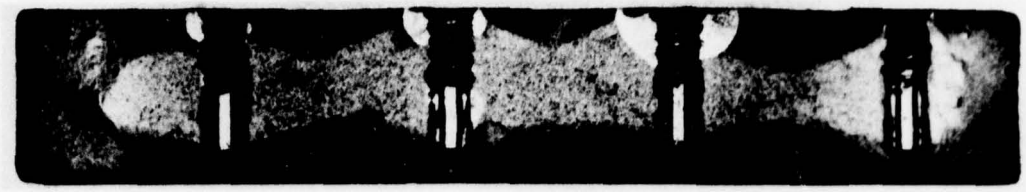

(a) Type E1 – specimen no. BJ14F

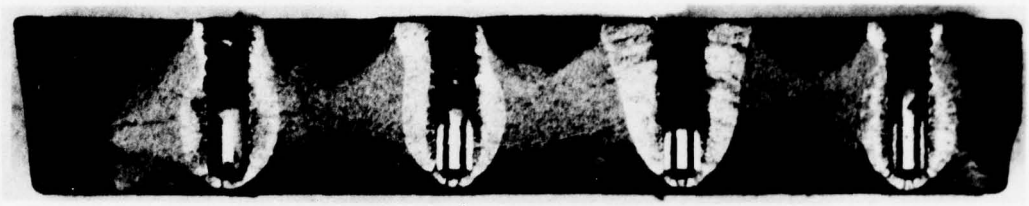

(b) Type E1 – specimen no. BJ7C

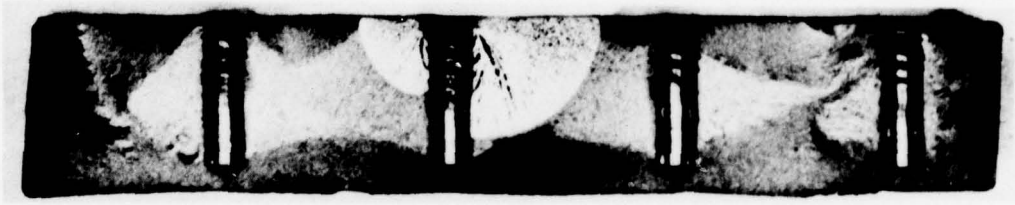

(c) Type E1 – specimen no. BJ11E

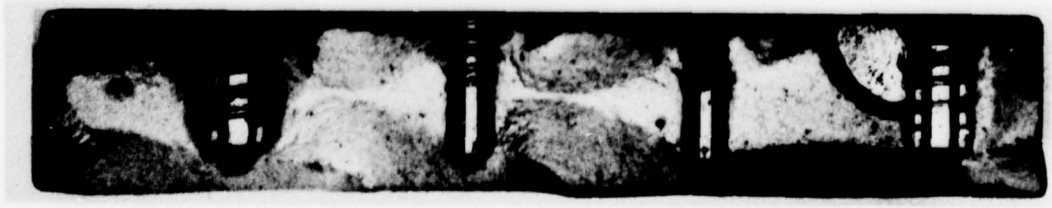

(d) Type G – specimen no. BJ12G

FIG. 4 EXAMPLES OF FATIGUE CRACKING

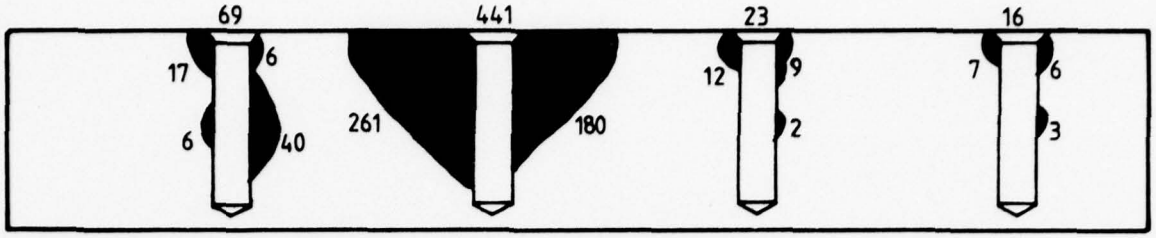

BJ 20D

Actual total fatigue area (T.F.A.) = $\frac{549}{4}$ = 137 mm^2

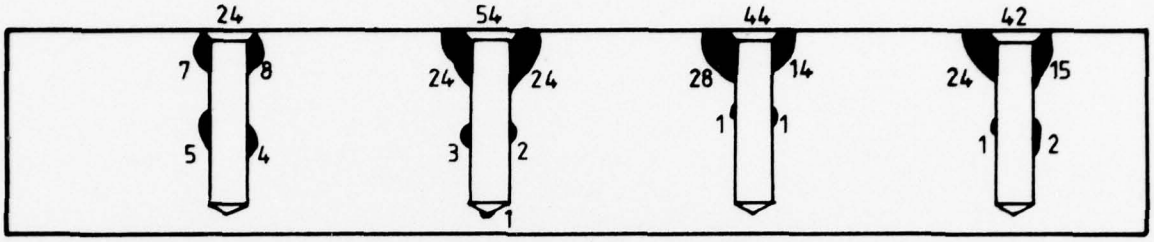

BJ 15C

T.F.A. = $\frac{164}{4}$ = 41 mm^2

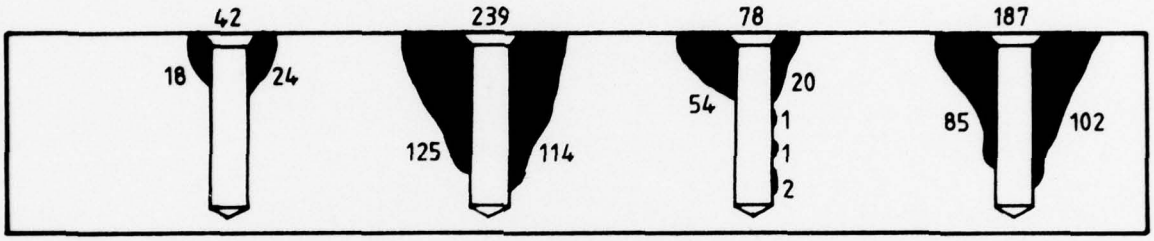

BJ 13I

T.F.A. = $\frac{546}{4}$ = 136 mm^2

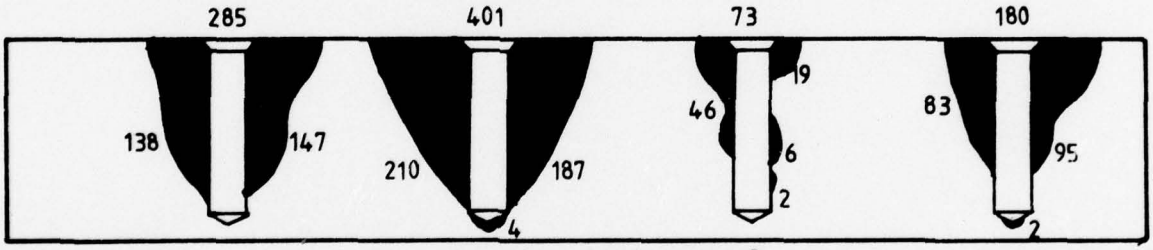

CL 25I

T.F.A. = $\frac{939}{4}$ = 235 mm^2

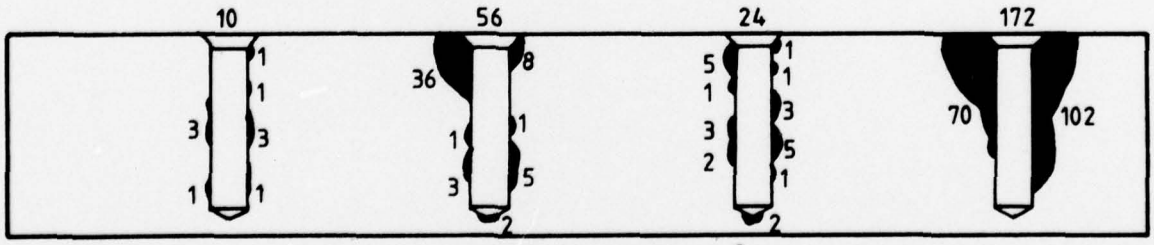

CL 21C

T.F.A. = $\frac{262}{4}$ = 66 mm^2

Note – Figures on diagrams refer to areas at 2X linear magnification.

FIG. 5a EXTENT OF FATIGUE CRACKING – TYPE E1 SPECIMENS (x2)

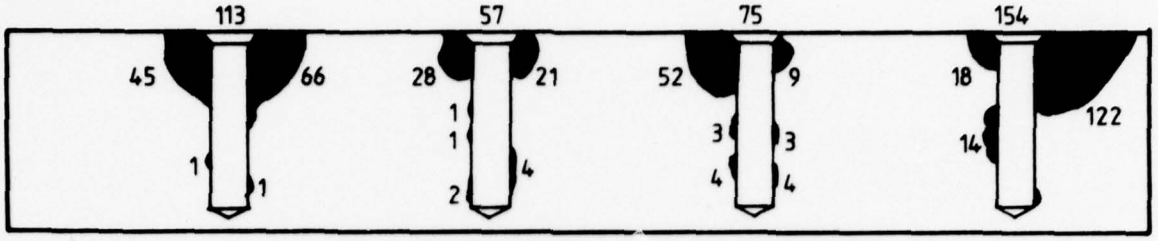

CL 22F Actual total fatigue area (T.F.A.) = $\frac{399}{4}$ = 100 mm^2

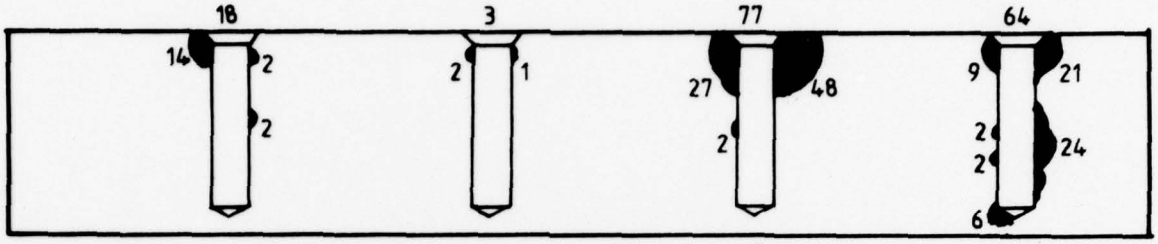

BJ 18H T.F.A. = $\frac{162}{4}$ = 40 mm^2

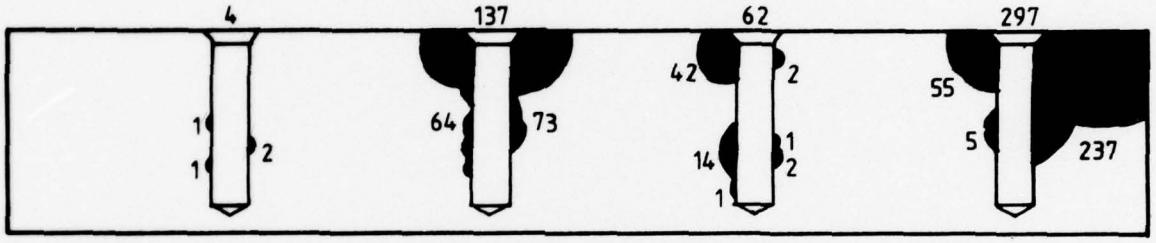

CL 27G T.F.A. = $\frac{500}{4}$ = 125 mm^2

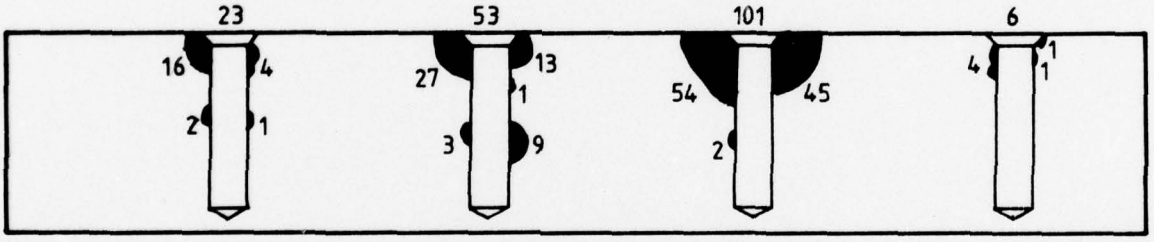

BJ 14F T.F.A. = $\frac{183}{4}$ = 46 mm^2

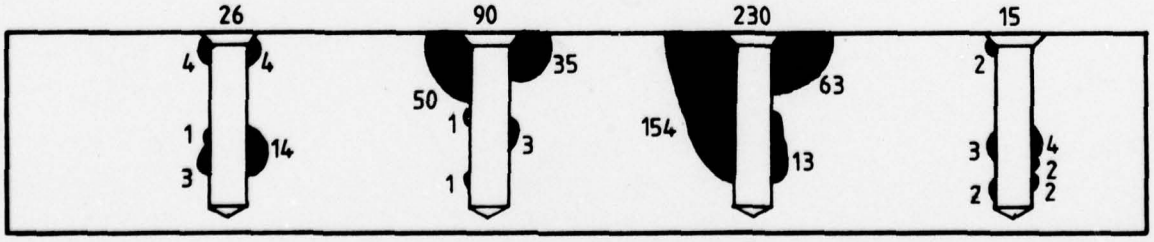

CL 26C T.F.A. = $\frac{361}{4}$ = 90 mm^2

Note — Figures on diagrams refer to areas at 2X linear magnification.

FIG. 5b

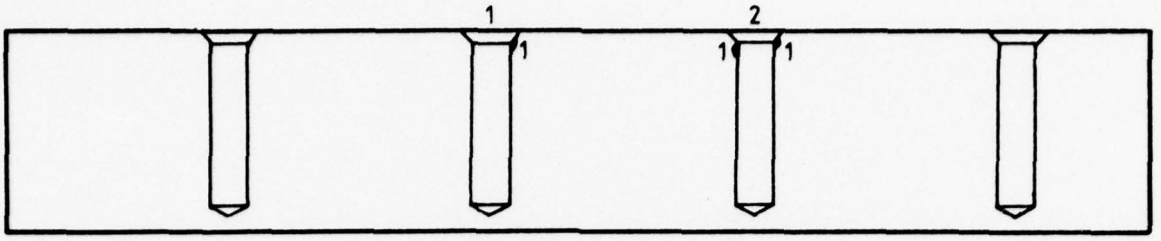

BJ 18F Actual total fatigue area (T.F.A.) = $\frac{3}{4}$ = 1 mm^2

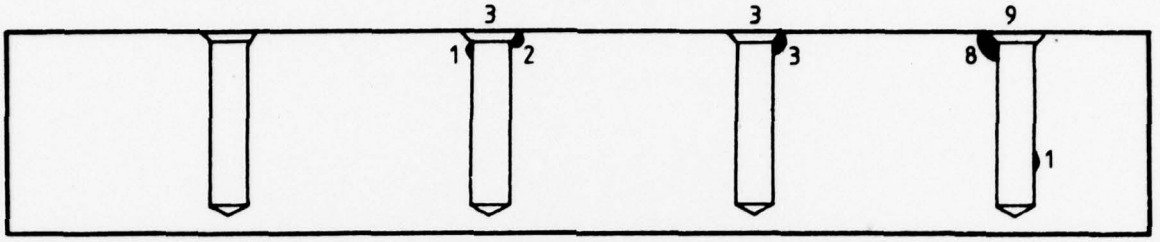

BJ 12F T.F.A. = $\frac{15}{4}$ = 4 mm^2

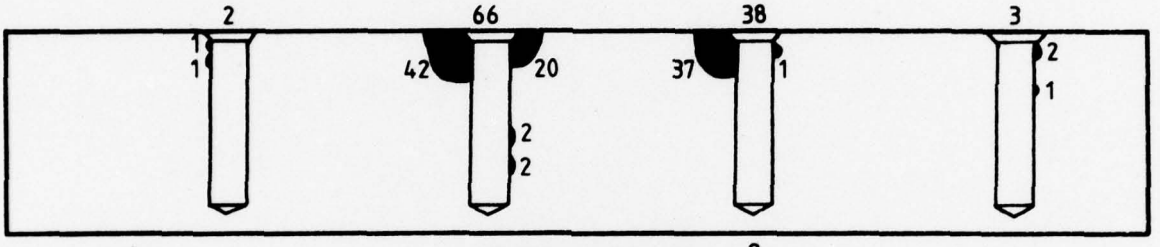

BJ 16D T.F.A. = $\frac{107}{4}$ = 27 mm^2

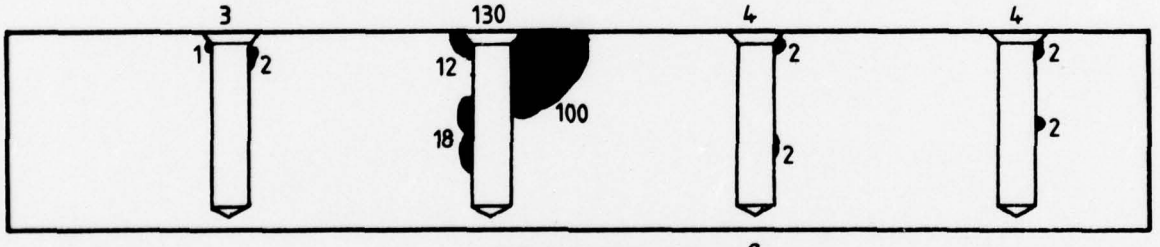

CL 21I T.F.A. = $\frac{141}{4}$ = 35 mm^2

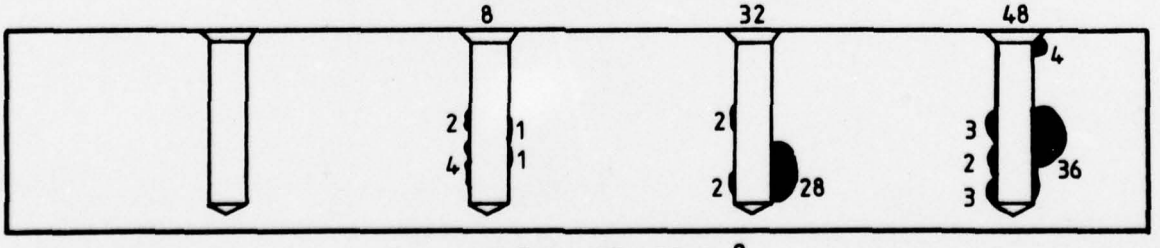

CL 24F T.F.A. = $\frac{88}{4}$ = 22 mm^2

Note – Figures on diagrams refer to areas at 2X linear magnification.

FIG. 5c

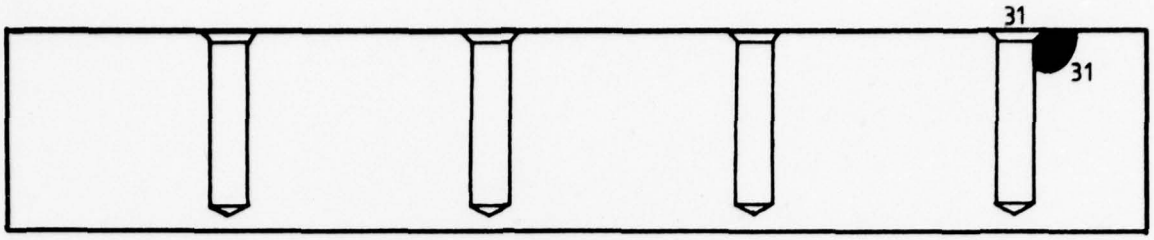

BJ 19E Actual total fatigue area (T.F.A.) = $\frac{31}{4}$ = 8 mm^2

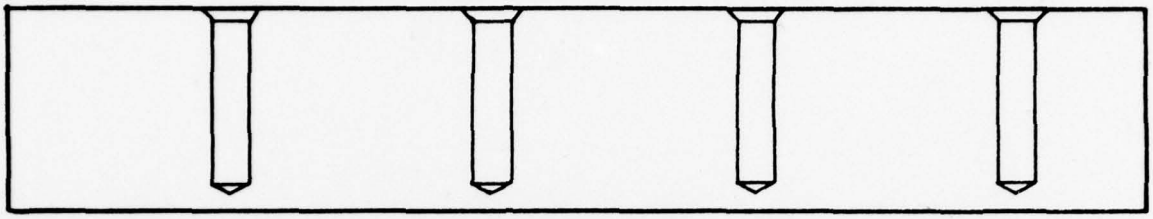

BJ 20F No cracks

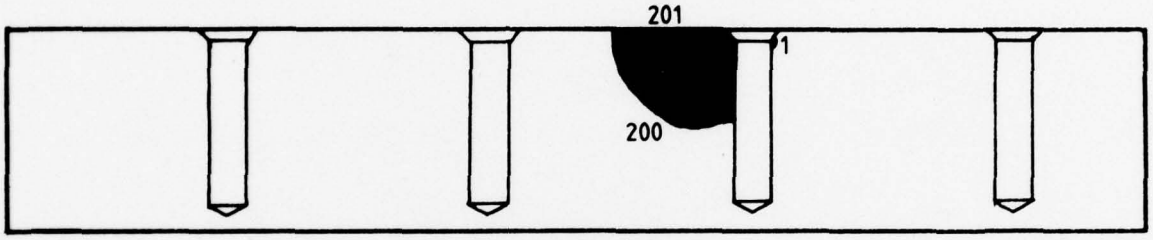

CL 25G T.F.A. = $\frac{201}{4}$ = 50 mm^2

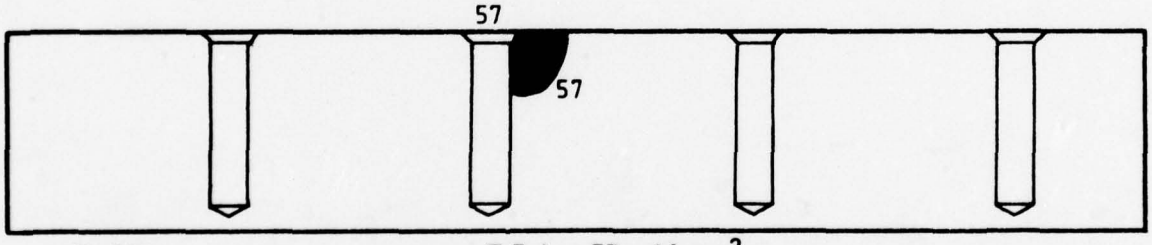

CL 24B T.F.A. = $\frac{57}{4}$ = 14 mm^2

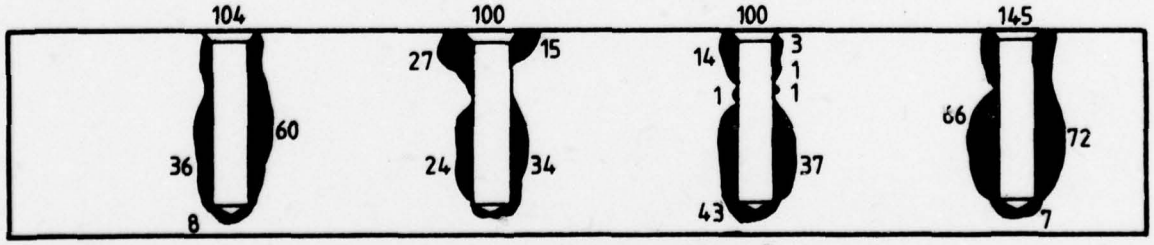

BJ 4H T.F.A. = $\frac{449}{4}$ = 112 mm^2

Note – Figures on diagrams refer to areas at 2X linear magnification.

FIG. 5d

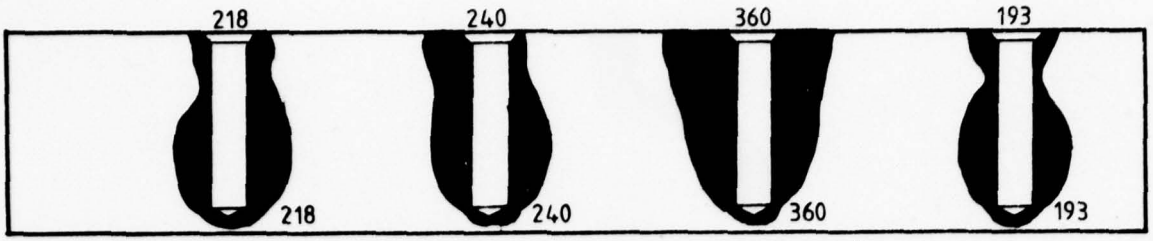

BJ 7C Actual total fatigue area (T.F.A.) = $\frac{1011}{4}$ = 253 mm^2

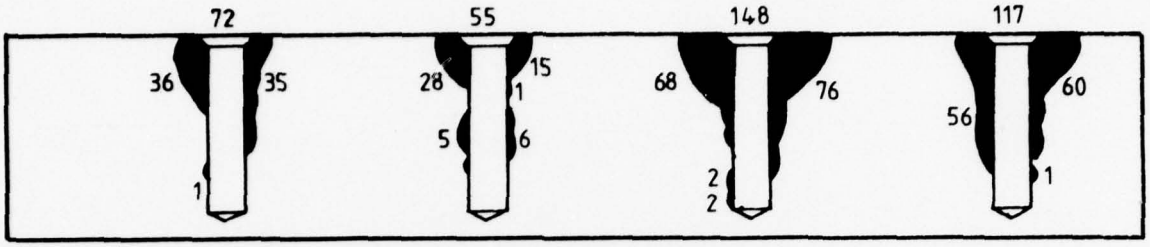

CL 23G T.F.A. = $\frac{392}{4}$ = 98 mm^2

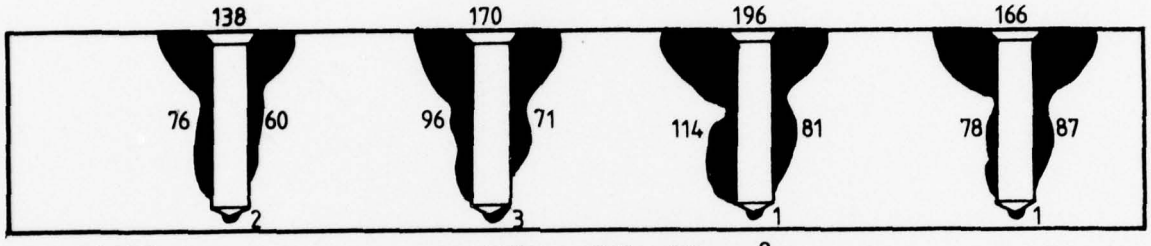

BJ 10F T.F.A. = $\frac{670}{4}$ = 168 mm^2

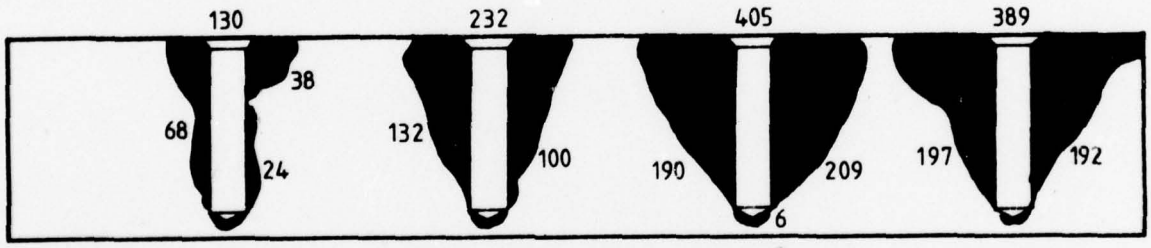

CL 21E T.F.A. = $\frac{1156}{4}$ = 289 mm^2

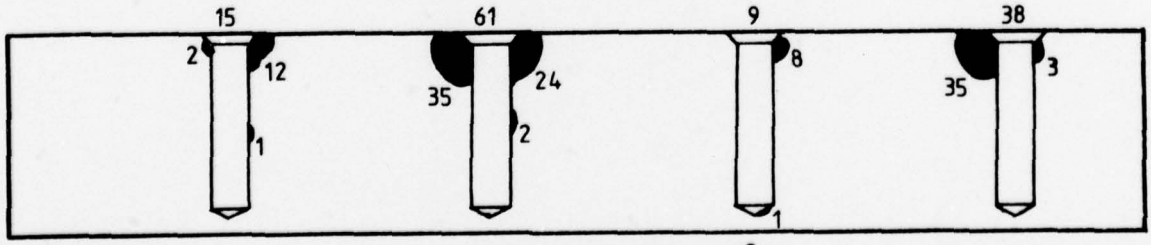

BJ 14B T.F.A. = $\frac{123}{4}$ = 31 mm^2

Note – Figures on diagrams refer to areas at 2X linear magnification.

FIG. 5e

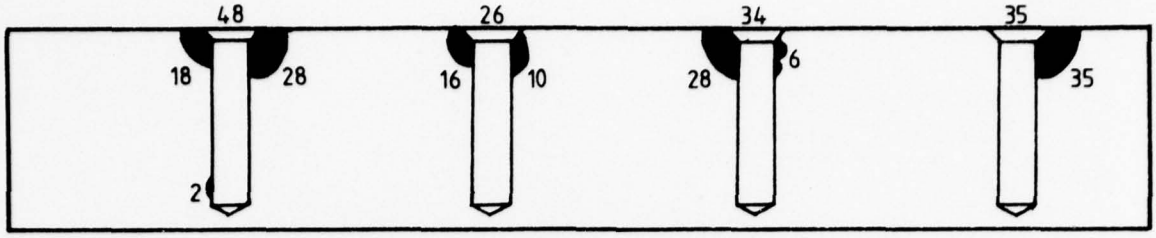

BJ 16J Actual total fatigue area (T.F.A.) = $\frac{143}{4}$ = 36 mm^2

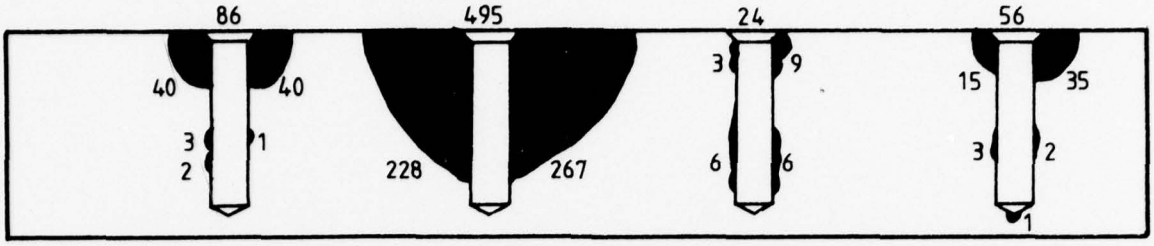

CL 26H T.F.A. = $\frac{661}{4}$ = 165 mm^2

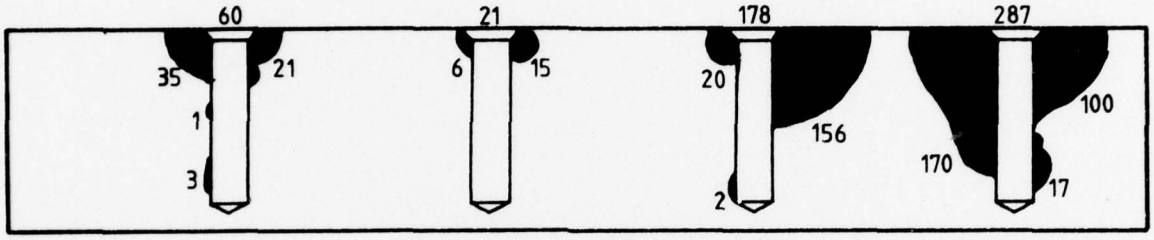

CL 22H T.F.A. = $\frac{546}{4}$ = 137 mm^2

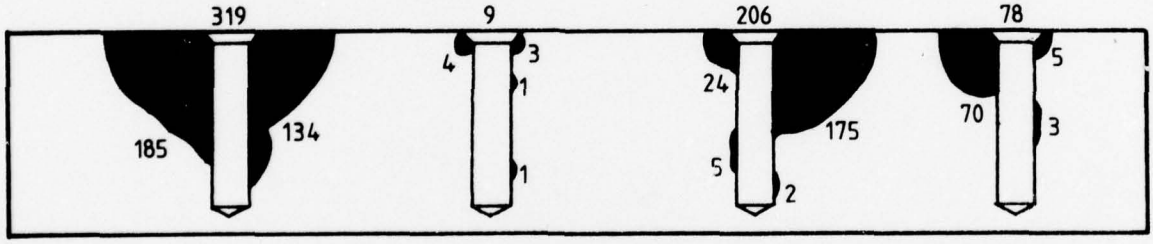

CL 23E T.F.A. = $\frac{612}{4}$ = 153 mm^2

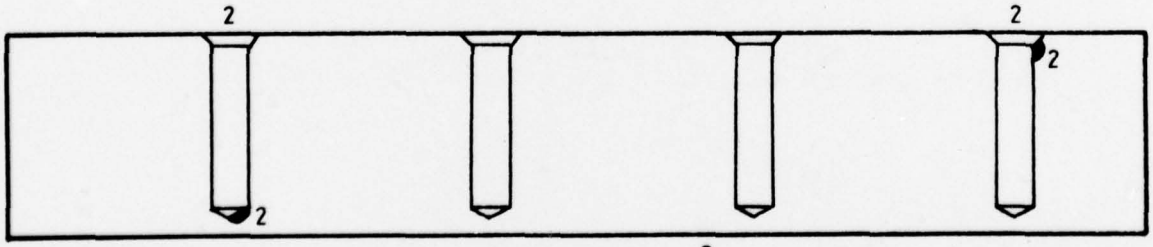

BJ 1D T.F.A. = $\frac{4}{4}$ = 1 mm^2

Note — Figures on diagrams refer to areas at 2X linear magnification.

FIG. 5f

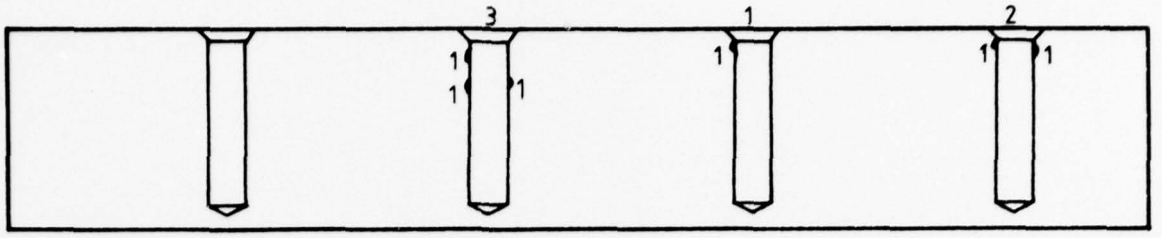

CL 22J Actual total fatigue area (T.F.A.) = $\frac{6}{4}$ = 2 mm^2

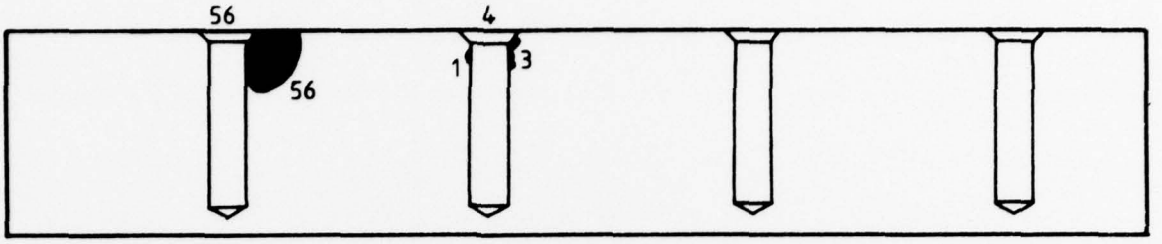

BJ 8H T.F.A. = $\frac{60}{4}$ = 15 mm^2

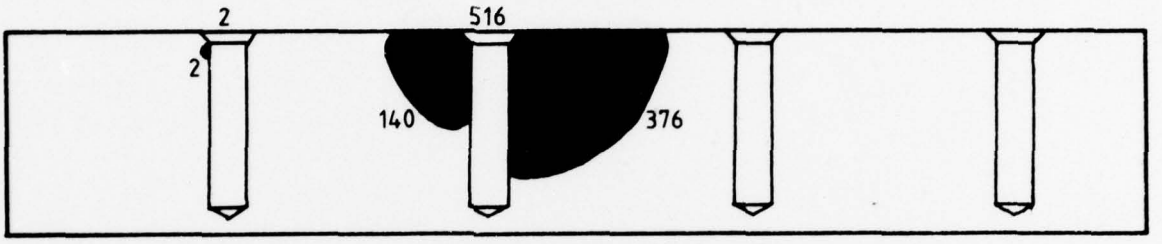

BJ 11E T.F.A. = $\frac{518}{4}$ = 130 mm^2

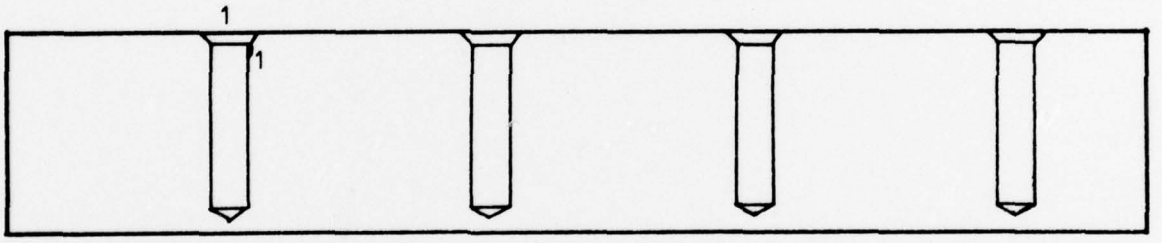

BJ 19C T.F.A. ≙ 0

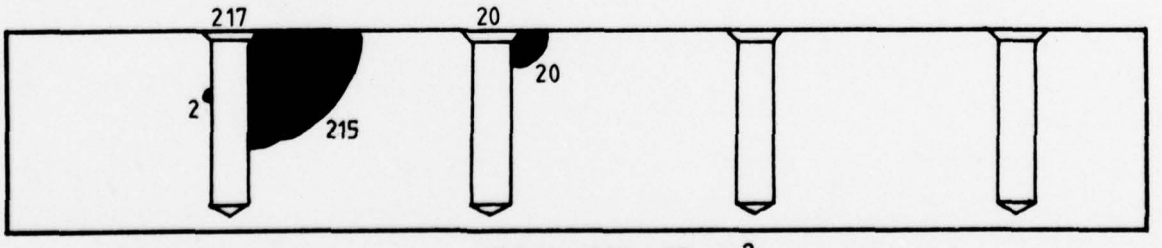

BJ 13C T.F.A. = $\frac{237}{4}$ = 59 mm^2

Note – Figures on diagrams refer to areas at 2X linear magnification.

FIG. 5g

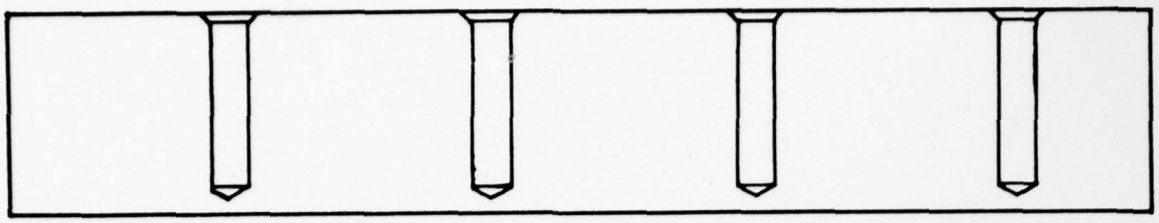

BJ 17I

No cracks

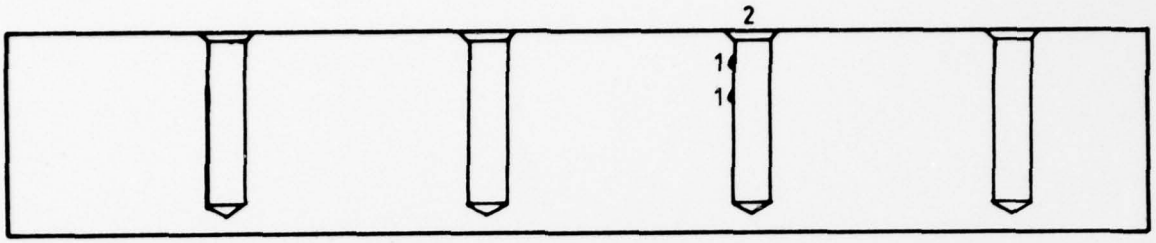

BJ 2I

T.F.A. = $\frac{2}{4}$ = 1 mm^2

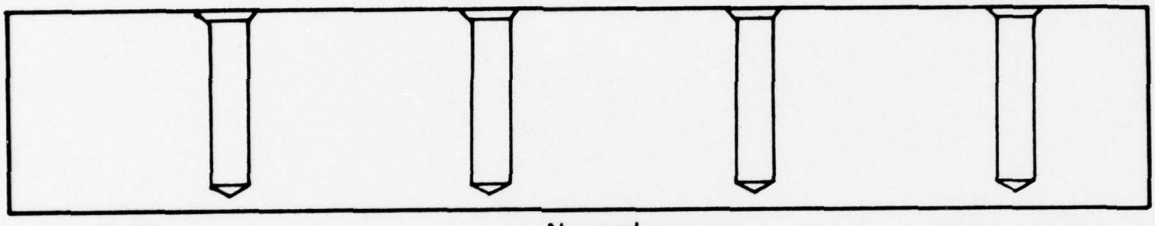

BJ 15I

No cracks

Note – Figures on diagrams refer to areas at 2X linear magnification.

FIG. 5h

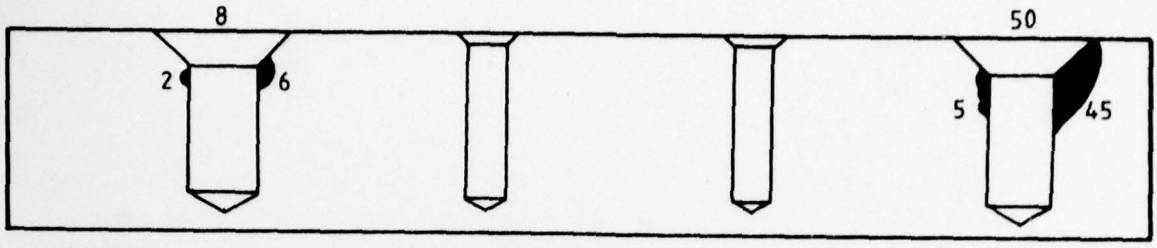

BJ 11J Actual total fatigue area (T.F.A.) = $\frac{58}{4}$ = 15 mm^2

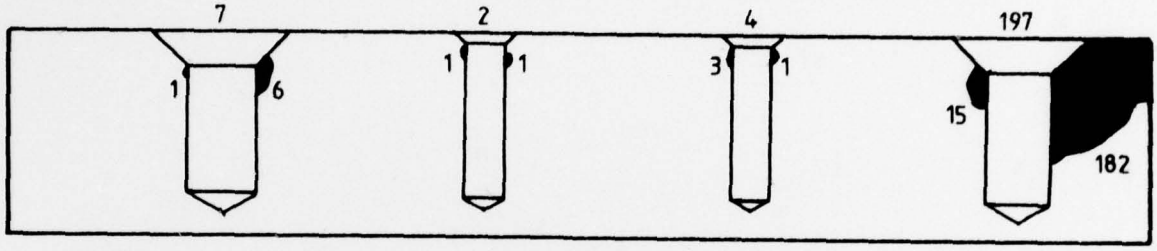

BJ 20I T.F.A. = $\frac{210}{4}$ = 53 mm^2

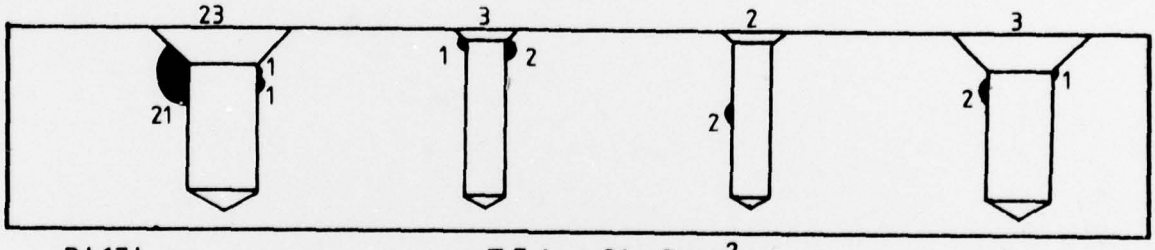

BJ 17J T.F.A. = $\frac{31}{4}$ = 8 mm^2

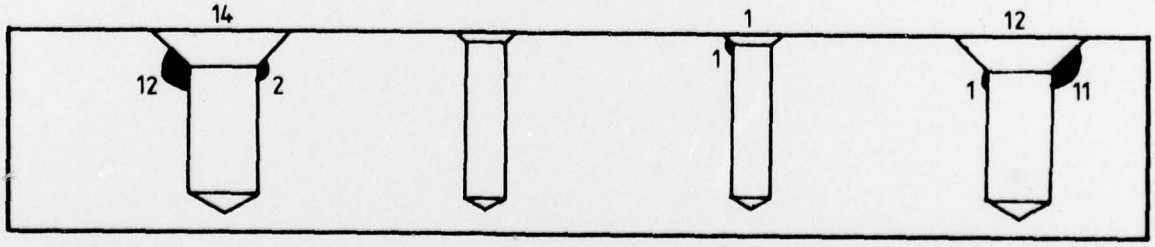

CL 24H T.F.A. = $\frac{27}{4}$ = 7 mm^2

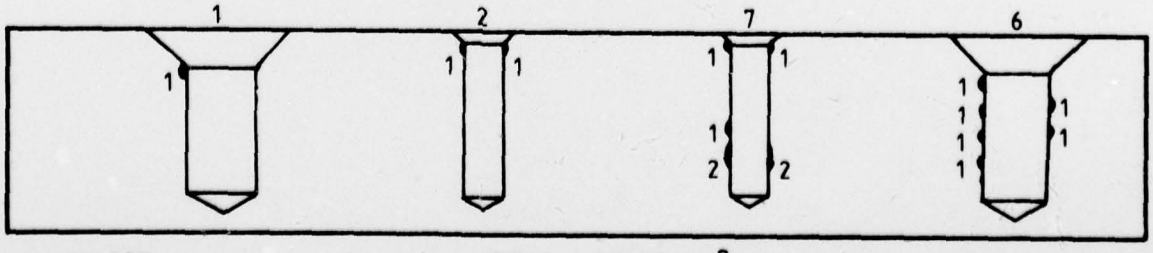

CL 23B T.F.A. = $\frac{16}{4}$ = 4 mm^2

Note – Figures on diagrams refer to areas at 2X linear magnification.

FIG. 6a EXTENT OF FATIGUE CRACKING – TYPE G SPECIMENS (x2)

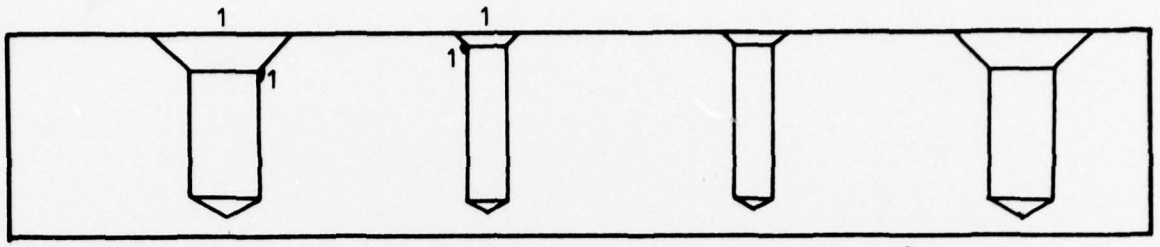

BJ 15H

Actual total fatigue area (T.F.A.) = $\frac{2}{4}$ = 1 mm^2

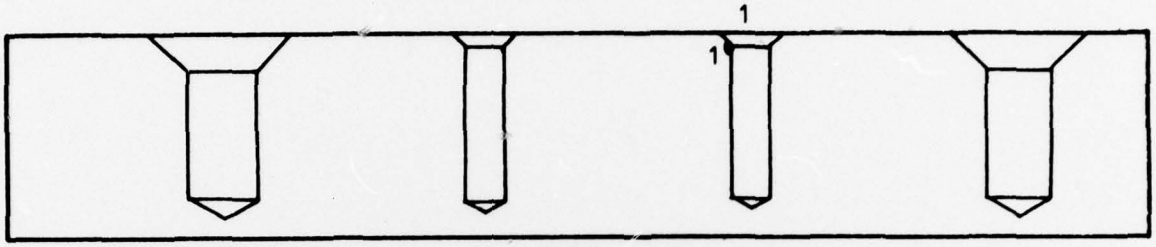

CL 27E

T.F.A. ≏ 0

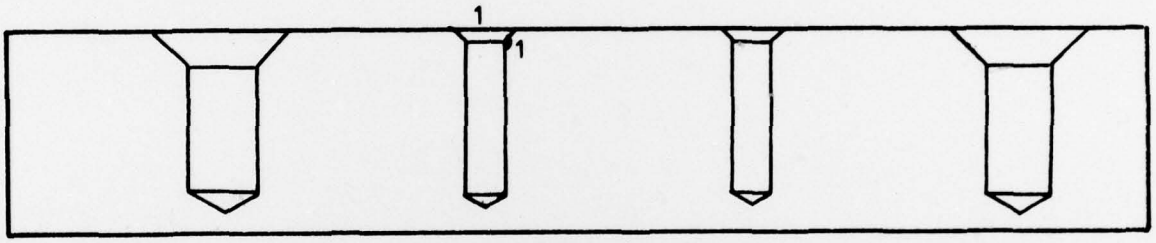

BJ 18E

T.F.A. ≏ 0

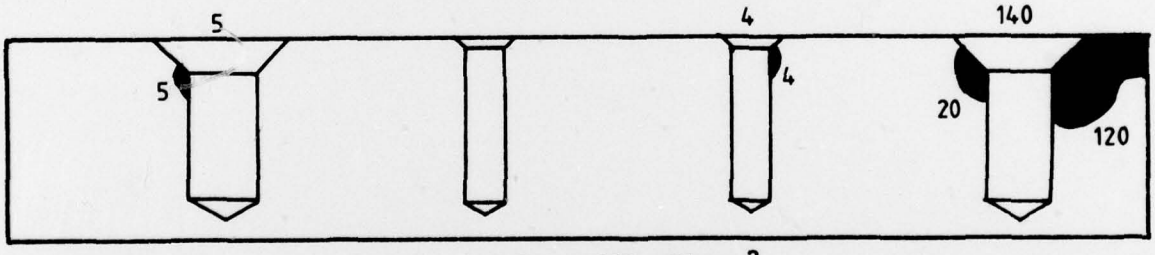

BJ 16E

T.F.A. = $\frac{149}{4}$ = 37 mm^2

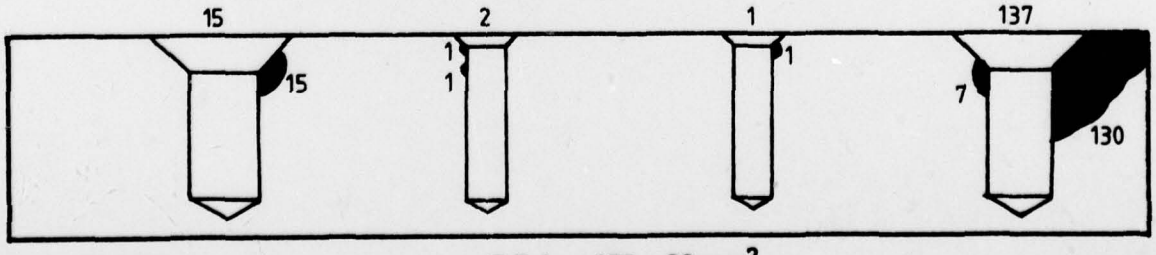

BJ 13D

T.F.A. = $\frac{155}{4}$ = 39 mm^2

Note – Figures on diagrams refer to areas at 2X linear magnification.

FIG. 6b

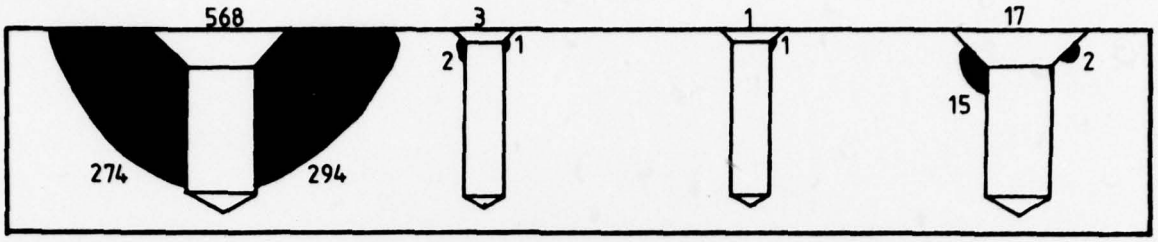

CL 21J

Actual total fatigue area (T.F.A.) = $\frac{589}{4}$ = 147 mm^2

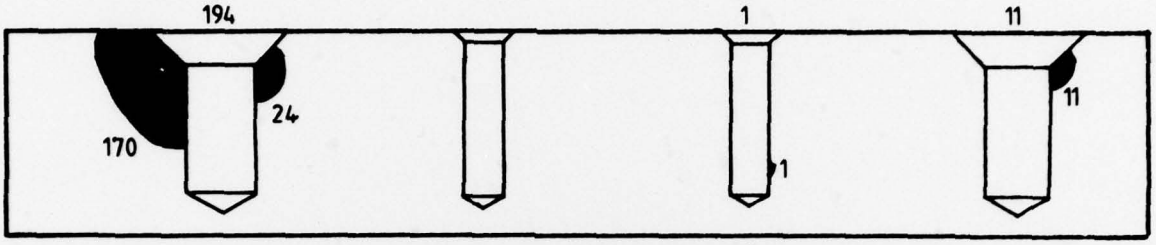

BJ 19B

T.F.A. = $\frac{206}{4}$ = 52 mm^2

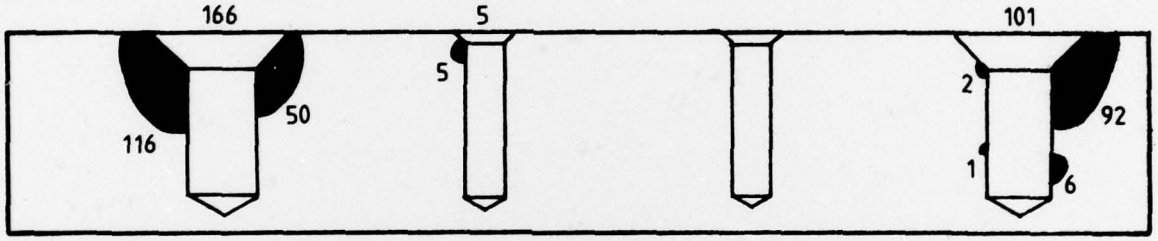

CL 22E

T.F.A. = $\frac{272}{4}$ = 68 mm^2

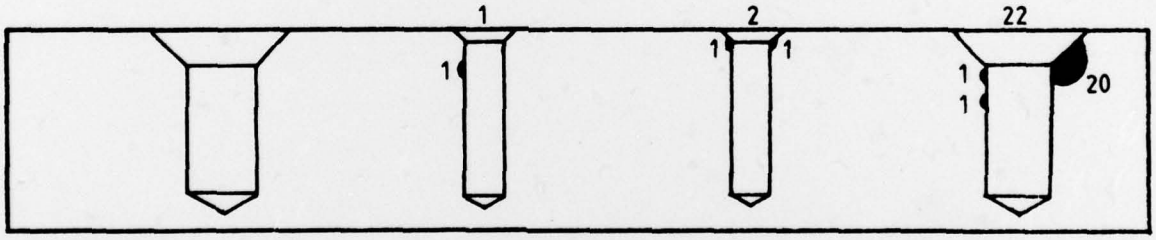

CL 21D

T.F.A. = $\frac{25}{4}$ = 6 mm^2

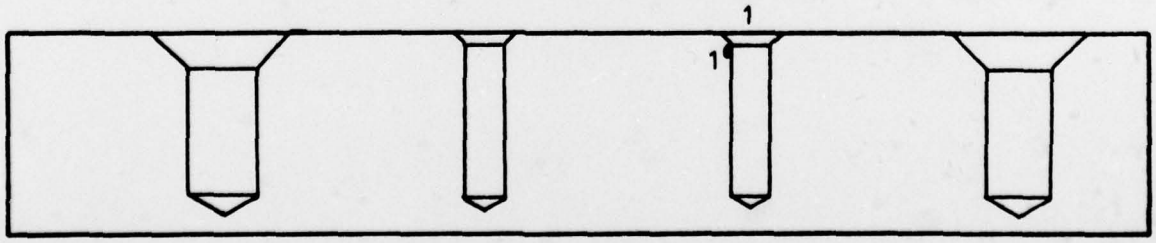

CL 26I

T.F.A. ≏ 0

Note — Figures on diagrams refer to areas at 2X linear magnification.

FIG. 6c

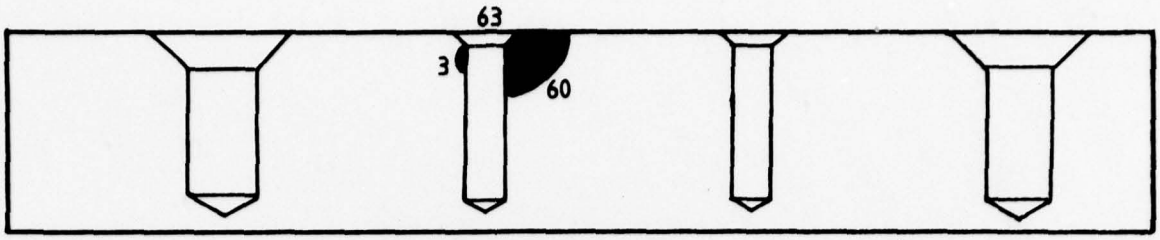

BJ 8I

Actual total fatigue area (T.F.A.) = $\frac{63}{4}$ = 16 mm^2

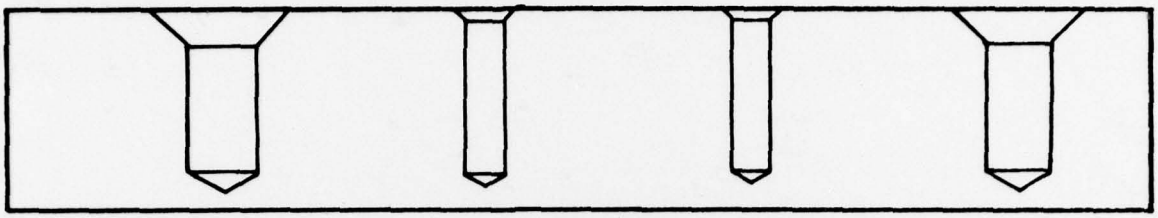

CL 25D

No cracks

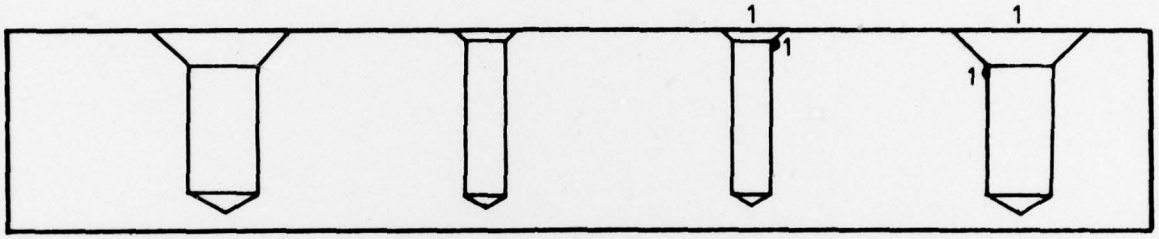

BJ 14G

T.F.A. = $\frac{2}{4}$ = 1 mm^2

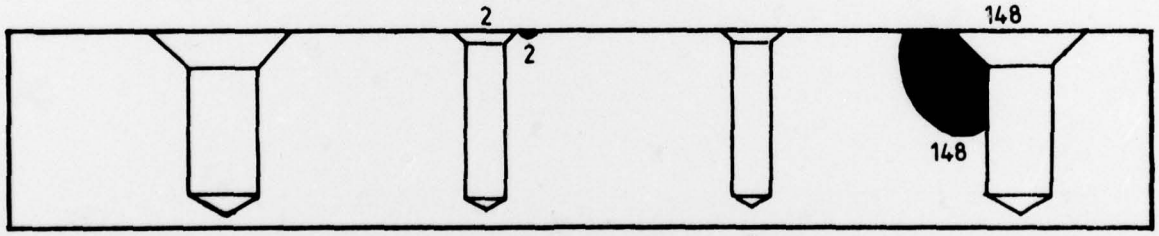

BJ 12G

T.F.A. = $\frac{150}{4}$ = 38 mm^2

Note – Figures on diagrams refer to areas at 2X linear magnification.

FIG. 6d

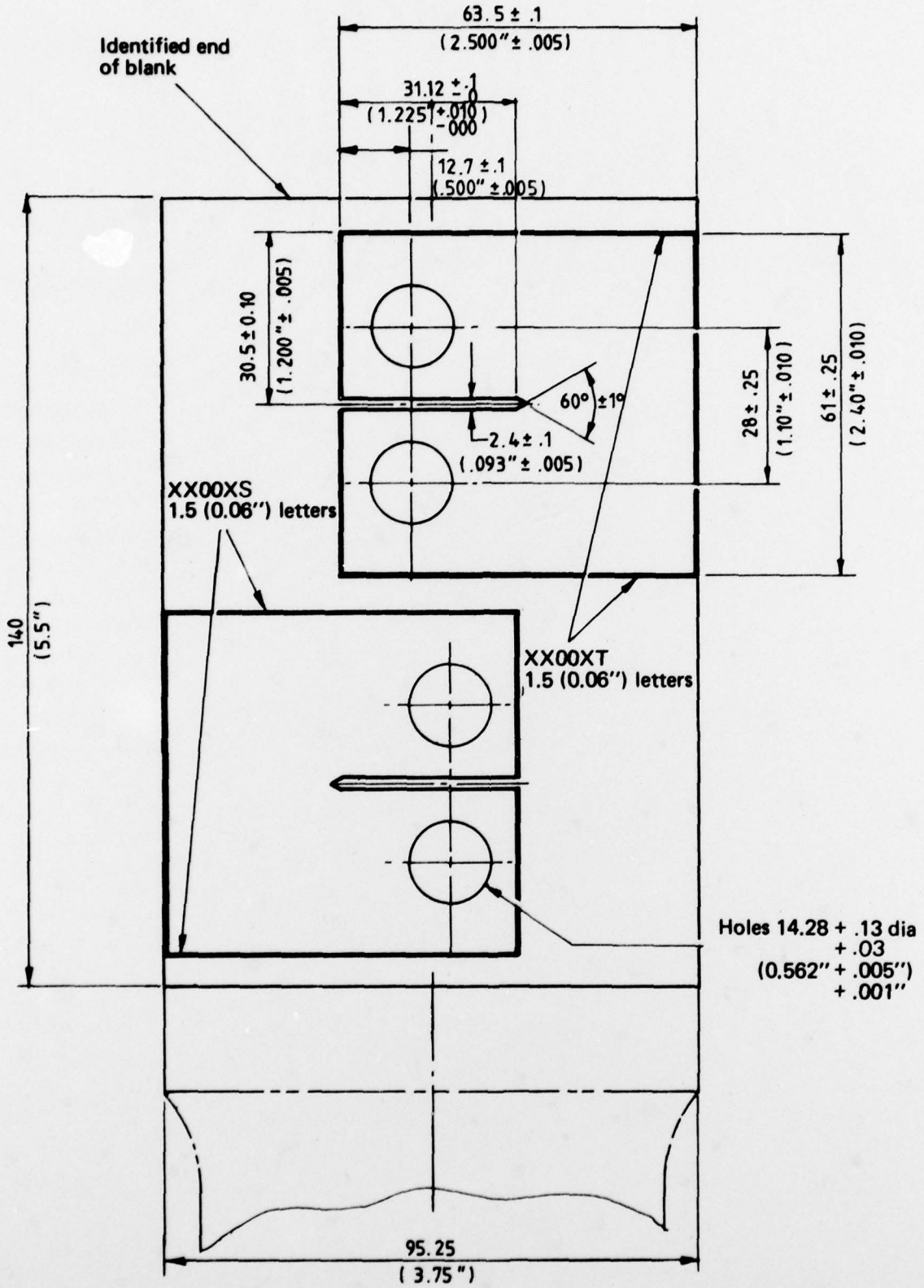

FIG. 7 LOCATION OF FRACTURE TOUGHNESS SPECIMENS

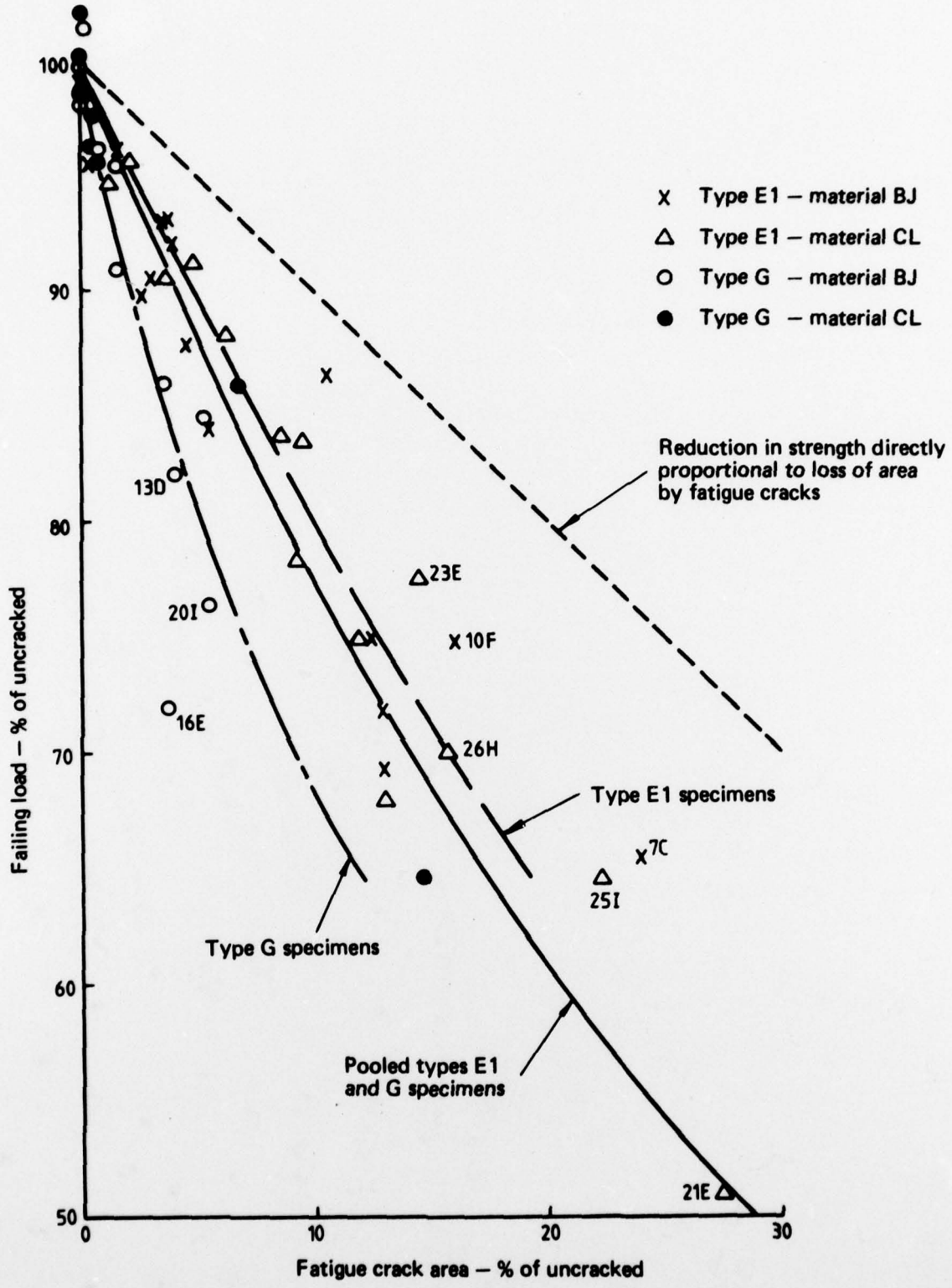

FIG. 8 RELATIONSHIP BETWEEN RESIDUAL STRENGTH AND FATIGUE CRACKED AREA

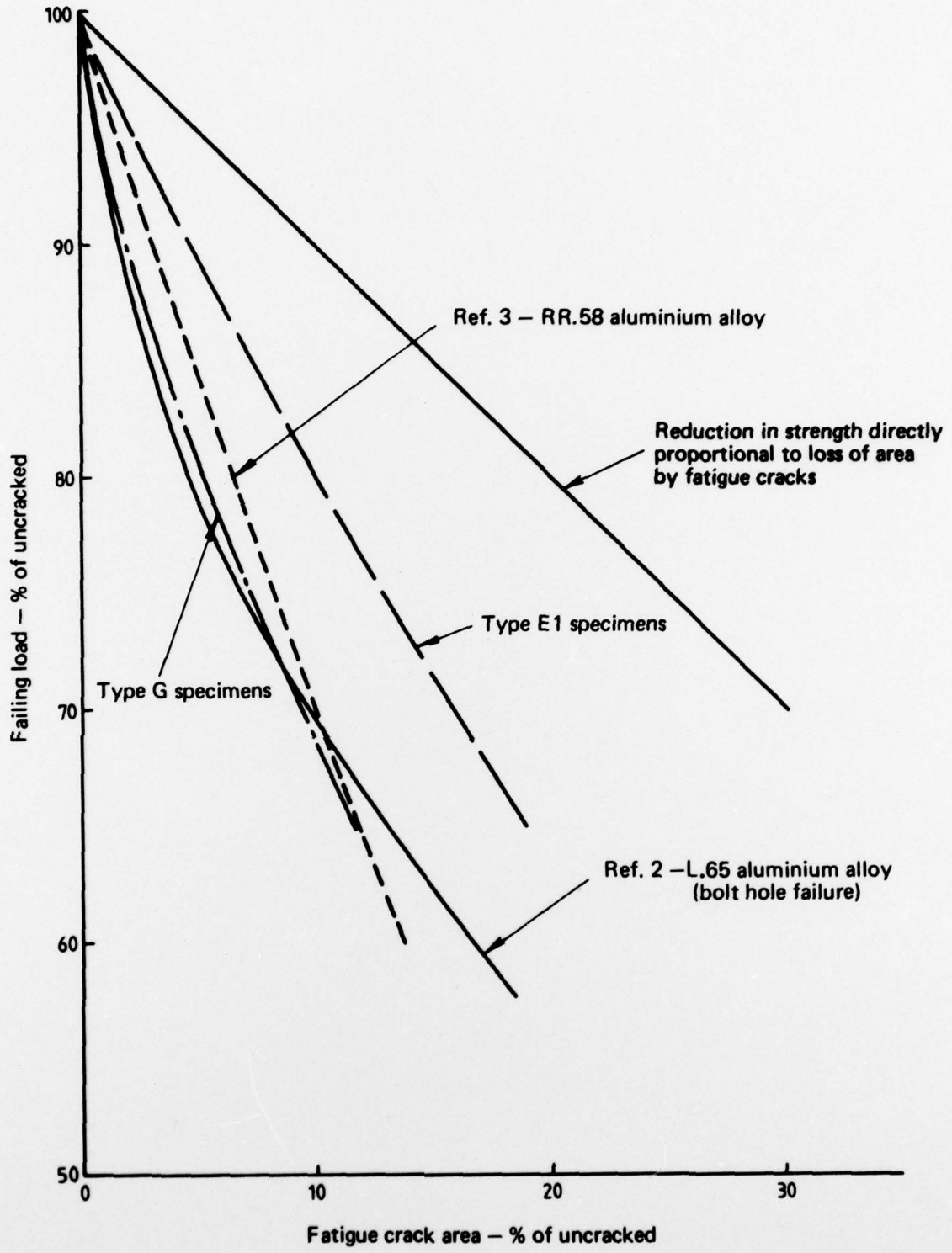

FIG. 9 COMPARISON OF PRESENT DATA WITH THAT ON BOLTED JOINTS

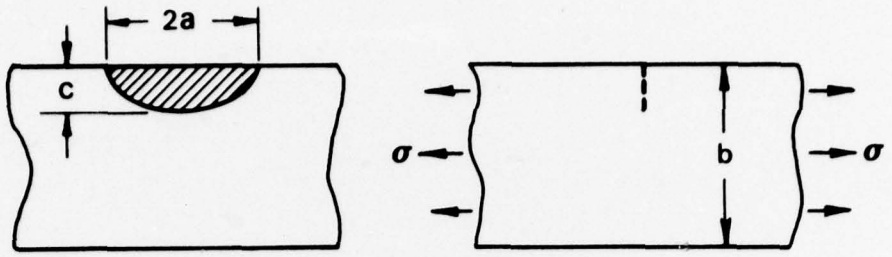

$$K_O = \sigma\sqrt{\pi c}$$

Where K_O is derived from the ratio $\frac{K_{IC}}{K_O}$ in Fig. 186 of Ref. 4

(a) Semi-elliptical surface crack in a slab (Ref. 4)

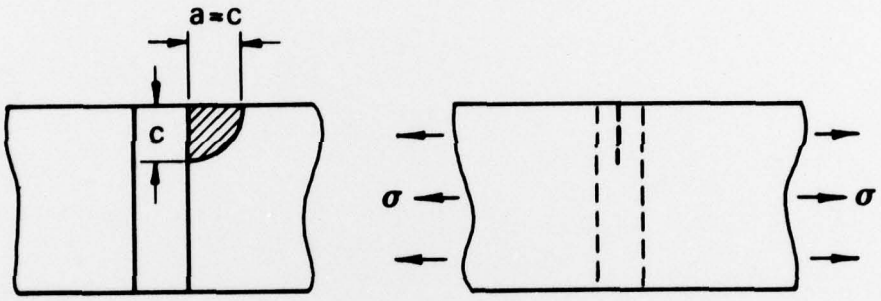

$$K_{IC} = \sigma\sqrt{2a}$$

(b) Semi-circular corner crack at a hole (Ref. 5)

FIG. 10 STRESS INTENSITY MODELS

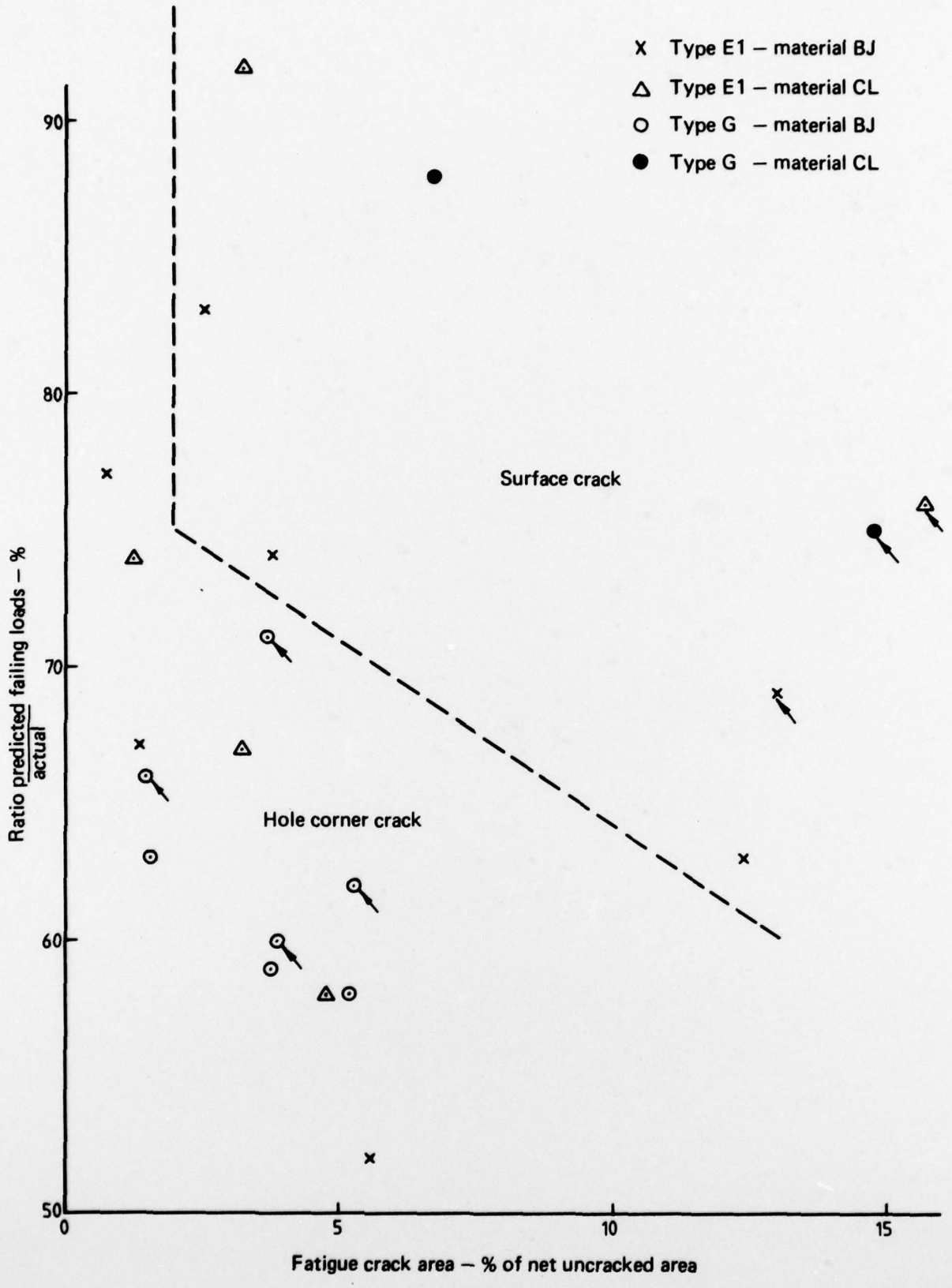

FIG. 11 PREDICTION OF RESIDUAL STRENGTH

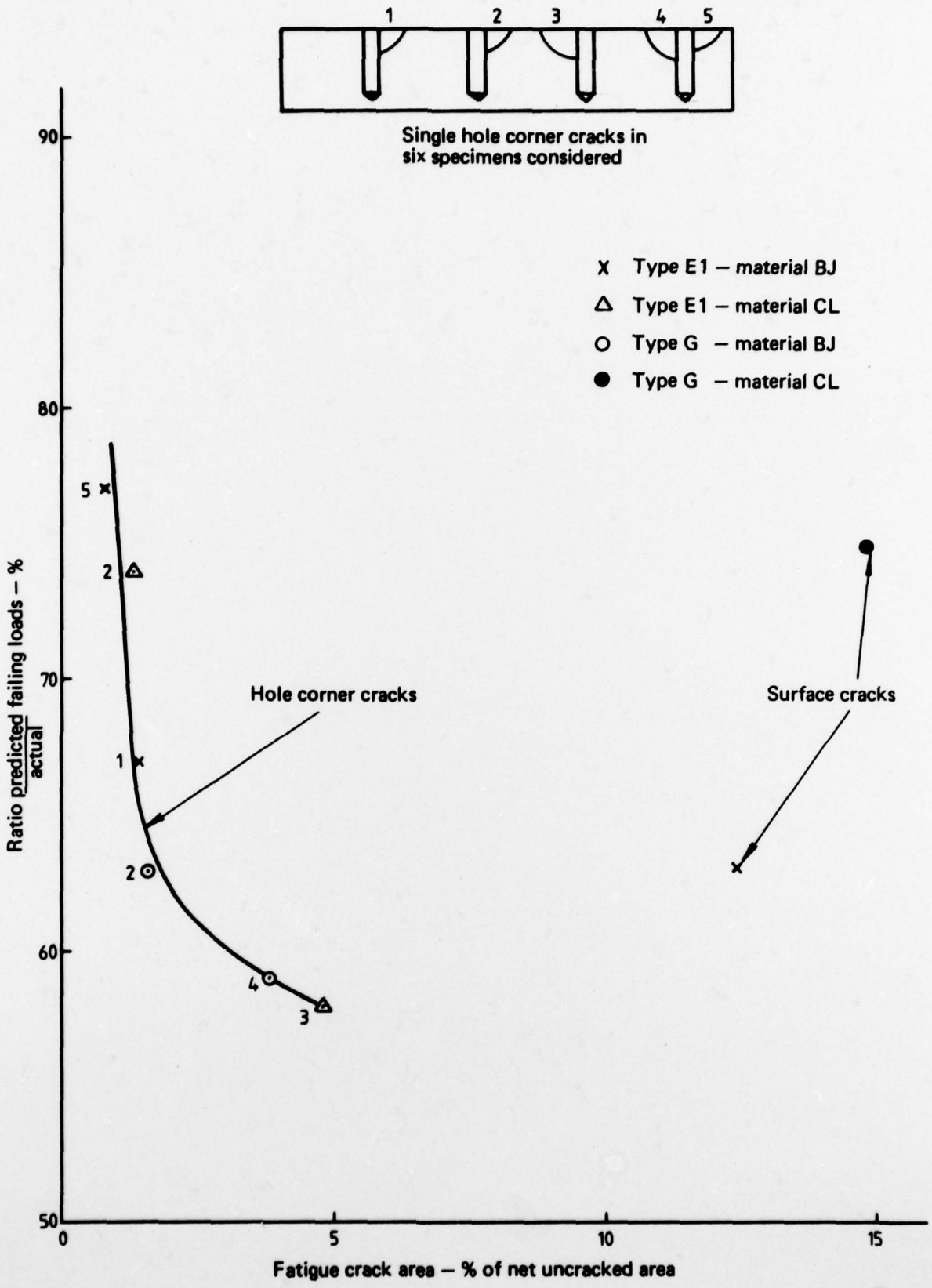

FIG. 12 PREDICTION OF RESIDUAL STRENGTH – 'SINGLE CRACK' CASES

DISTRIBUTION

AUSTRALIA	Copy No.
DEPARTMENT OF DEFENCE	
Central Office	
Chief Defence Scientist	1
Executive Controller, ADSS	2
Superintendent, Defence Science Administration	3
Defence Library	4
JIO	5
Assistant Secretary, DISB	6–20
Aeronautical Research Laboratories	
Chief Superintendent	21
Superintendent, Structures Division	22
Divisional File, Structures Division	23
Authors: J. Y. Mann	24
F. G. Harris	25
G. W. Revill	26
Library	27
B. C. Hoskin	28
C. A. Patching	29
A. O. Payne	30
Materials Research Laboratories	
Library	31
Weapons Research Establishment	
Library	32
Central Studies Establishment	
Library	33
Engineering Development Establishment	
Library	34
RAN Research Laboratory	
Library	35
Air Force Office	
Library, Aircraft Research and Development Unit	36
Air Force Scientific Adviser	37
Library, Engineering (CAFTS) Branch	38
D. Air Eng. Canberra	39
H.Q. Support Command (SENGSO)	40
Army Office	
Army Scientific Adviser	41
Royal Military College	42
US Army Standardisation Group	43
Navy Office	
Naval Scientific Adviser	44